The Astronomical Journal, 164:199 (19pp), 2022 November https://doi.org/10.3847/1538-3881/ac90c9

The Orbits of the Main Saturnian Satellites, the Saturnian System Gravity Field, and the Orientation of Saturn's Pole*

Robert. A. Jacobson
Jet Propulsion Laboratory, California Institute of Technology, 4800 Oak Grove Drive, Pasadena, CA 91109-8099, USA; robert.a.jacobson@jpl.nasa.gov
Received 2022 June 13; revised 2022 August 15; accepted 2022 September 7; published 2022 October 18

Abstract

Four spacecraft have been sent to investigate the Saturnian system: Pioneer 11, Voyager 1, Voyager 2, and Cassini. By analyzing data acquired with these spacecraft together with Earth-based and Hubble Space Telescope satellite astrometry and Saturnian ring and satellite occultations, we constructed a model for the orientation and precession of Saturn's pole and determined gravitational parameters of the system and the orbits of the Saturnian satellites. This article provides details of our analysis and its results.

Unified Astronomy Thesaurus concepts: Saturnian satellites (1427)

1. Introduction

As of 2022 January 1, 82 satellites have been found to orbit Saturn. We group them into the 8 main satellites (Mimas, Enceladus, Tethys, Dione, Rhea, Hyperion, Titan, Iapetus), the 15 minor satellites (Janus, Epimetheus, Helene, Telesto, Calypso, Atlas, Prometheus, Pandora, Pan, Methone, Pallene, Polydeuces, Daphnis, Anthe, Aegaeon), and the 59 irregular satellites (small bodies orbiting Saturn at distances well beyond the main satellites, too numerous to be listed). For the work described in this article our satellite system is composed of only the main satellites, five minor satellites, and one irregular satellite. The omitted satellites are too small to have a significant dynamical effect on that system. Their orbits will be the subject of future analyses that will incorporate the results of this work.

Pioneer 11 was the first spacecraft to reach Saturn (Fimmel et al. 1980). Shortly after its 1979 September encounter Null et al. (1981) used the Doppler tracking of the spacecraft together with Saturnian satellite orbit apse and node rate information in an analysis of the gravitational field of the Saturnian system. After Voyager 1 and Voyager 2 followed Pioneer 11 to Saturn, arriving in 1980 November and 1981 August, respectively (Morrison 1982), Campbell & Anderson (1989) extended the work of Null et al. Combining the Voyager Doppler tracking, radiometric range, and star–satellite imaging with the Pioneer data set, they revised the estimates for Saturn's gravity harmonics; improved the *GM* estimates of Saturn, Rhea, Titan, and Iapetus; and added a weak estimate of Tethys's *GM* (*GM* is the product of the Newtonian constant of gravitation *G* and the body's mass *M*).

In preparation for the Cassini tour, Jacobson (2004) repeated Campbell and Anderson's work with a more extensive spacecraft data set. He also replaced the analytical theory for the Saturnian satellite orbits used previously with a numerical integration of a full dynamical model that allowed observations of the gravitational interaction among the satellites to contribute directly to the determination of the gravity parameters. He extended the satellite system to the Lagrangian satellites, Helene, Telesto, and Calypso, because their dynamics provide direct information on the *GM*s of Tethys and Dione (Dermott & Murray 1981). He estimated the satellite orbits and gravity parameters with an extensive set of satellite astrometry from Earth-based observatories and the Hubble Space Telescope (HST), together with the spacecraft data.

Cassini entered orbit around Saturn on 2004 July 1 and successfully completed its 4 yr Prime mission, its Equinox mission extension to 2010, and its Solstice second mission extension to 2017. The tour of the Saturnian system ended in a series of "Ring-Grazing" and "Grand Finale" orbits and a final "Plunge" into Saturn's atmosphere on 2017 September 17 (Spilker 2019). At the start of the approach of Cassini to Saturn, we began updating the work of Jacobson (2004) by incorporating the Cassini Doppler tracking, radiometric range, and imaging data and adding new Earth-based and HST satellite astrometry as it became available. We also added Phoebe to our satellite system because a refined orbit was needed to support the Cassini flyby of that satellite. To aid in the determination of the orientation of Saturn's pole, we began processing Saturn ring occultation measurements from both Earth and spacecraft (French et al. 1993). The discovery of the satellite Methone (Porco et al. 2005) prompted us to expand our satellite system. Mimas strongly perturbs Methone's orbit, and Cassini imaging observations of Methone enabled us to refine the Mimas *GM* determination (Jacobson et al. 2006b). Jacobson et al. (2006a) reported the results of our early analysis involving Cassini data. Later, we expanded the system yet again, adding the fourth Lagrangian satellite, Polydeuces, that was discovered by the Cassini Imaging Team (Porco & the Cassini Imaging Team 2004). Throughout the Cassini tour we continued to improve our model of the satellite orbits, gravity field, and pole orientation and to convey those improvements to the Cassini Project to aid in the spacecraft navigation. This article reports the results of our final post-Cassini analysis.

2. Satellite Orbit Model

The model for the orbits of the satellites is a numerical integration of their equations of motion (Peters 1981) augmented with the effects of the Saturnian rings (Krogh et al. 1982),

* ©2022 California Institute of Technology. Government sponsorship acknowledged.

Table 1
Gravitational Constants

Name	Value (km^3 s^{-2})	Source
Jovian system *GM*	126,712,761.8414	R. A. Jacobson (2021, private communication)
Uranian system *GM*	5,794,556.4000	Park et al. (2021)
Neptunian system *GM*	6,836,527.1006	Park et al. (2021)
Sun *GM*[a]	132,713,233,263.3514	Park et al. (2021)

Note.
[a] Includes the *GM*s of the inner planetary systems.

Table 2
Saturnian Ring Mass

Ring	R_{inner} (km)	R_{outer} (km)	*GM* (km^3 s^{-2})	References
C	74,500	92,000	0.0390 ± 0.0091	Hedman & Nicholson (2014)
B	92,000	117,500	0.7840 ± 0.2100	Hedman & Nicholson (2016)
Cass	117,500	122,357	0.0021 ± 0.0006	Colwell et al. (2009)
A	122,357	136,780	0.3000 ± 0.0901	Tiscareno et al. (2007)

Note. The quoted uncertainties are 1σ.

the tides raised on Saturn by the satellites and the tide raised on Enceladus by Saturn (Mignard 1979), and a post-Newtonian general relativistic correction (Moyer 1968) including the Lense–Thirring effect (Moyer 2000). Methone and the Lagrangian satellites, with the exception of Helene, are taken to be massless; their actual masses are undetermined but presumed to be quite small (Thomas et al. 2018). We include external perturbations from Jupiter, Uranus, Neptune, and the Sun but ignore the direct effects of the inner planets and the Moon. Instead, the *GM* of the Sun is increased by the *GM*s of the ignored bodies to indirectly account for their perturbations. We allow for the gravitational field of an oblate Saturn and for the quadrupole gravitational fields of seven of the eight main satellites; Hyperion is excluded because of its small size and chaotic rotation. We also account for the forced libration of Enceladus (Thomas et al. 2016) with an adaptation of the Phobos libration model (Jacobson 2010). The integration is performed in Cartesian coordinates centered at the Saturnian system barycenter and referred to the International Celestial Reference Frame (ICRF).

The inertial direction of Saturn's pole is needed to orient Saturn's gravity field. We obtain the pole direction from the numerical integration of its motion based on the rotational equations of motion for a rigid body. The equations assume that the planet is axially symmetric and that the torques applied are derived from the Sun, Jupiter, and seven satellites (Mimas, Enceladus, Tethys, Dione, Rhea, Titan, and Iapetus) acting on the planet's figure as represented by its zonal gravitational harmonics. Details of the pole model appear in the Appendix.

JPL planetary ephemeris DE440 (Park et al. 2021) provides the positions of the perturbing planets and Sun. Table 1 lists their *GM*s. The *GM*s of the satellites, the gravitational harmonics of the satellites and Saturn, its Love number, the orientation of its pole, and its axial moment of inertia are determined in the course of fitting the orbits to the observations. Table 2 contains the inner and outer ring radii and the ring *GM*s. We were unable to estimate improved values in our analysis.

3. Observational Data

To determine the parameters in our dynamical model, we analyzed an extensive set of observations that contained Pioneer 11 Doppler tracking; Voyager and Cassini Doppler tracking, radiometric range, and optical navigation and Imaging Science observations; Earth-based and HST satellite astrometry; Earth-based satellite transits; satellite mutual events (occultations and eclipses); satellite stellar occultations (reduced to astrometric positions); Saturn ring stellar occultations observed from Earth, from Voyager 2 with the Photopolarimeter (PPS) instrument, and from Cassini with the Visual and Infrared Mapping Spectrometer (VIMS) and Ultraviolet Imaging Spectrograph (UVIS) instruments; Saturn ring spacecraft occultations measured with the Voyager 1 and Cassini Radio Science Subsystem (RSS); Saturn ring plane position angles; and ring plane crossing timings.

The spacecraft tracking data were acquired via NASA's Deep Space Network (DSN). During the Cassini Grand Finale, some additional tracking was obtained from the European Space Agency (ESA) stations in New Norcia, Australia, and Malargue, Argentina. The Pioneer 11 tracking covers 16 days from 1979 August 20 to 1979 September 5. The Voyager 1 tracking data arc begins on 1980 August 7 and ends 105 days later on 1980 November 20. The 106-day arc for Voyager 2 spans 1981 June 8 to 1981 September 22. The Cassini tracking data arc is from 2004 February 6 to 2017 September 15. For the most part we used coherent two-way Doppler, but when it was unavailable, i.e., when the round-trip light time prevented the tracking station that was transmitting the radio signal from also receiving it, we occasionally acquired coherent three-way Doppler or noncoherent one-way Doppler. Doppler was generally compressed at 1-minute intervals, although for Cassini a 30 s compression was used during some of the satellite flybys to enhance the gravity analysis. Shorter compression times have been found to be subject to numerical noise when processed (Mackenzie 2006) and were avoided.

We corrected the tracking data for all four spacecraft for Earth media effects with a seasonal troposphere model and an ionosphere model. For Cassini we also applied daily weather

adjustments, when available, to the troposphere model during some of the periods of close satellite flybys (Bar-Sever et al. 2007). The Voyager and Cassini three-way data were calibrated for DSN interstation clock offsets. The one-way data were adjusted to allow for a bias and drift in the spacecraft's onboard ultrastable oscillator (USO). The Pioneer 11 and Voyager tracking was at S band, but the Voyager spacecraft also have X-band downlink capability. Differences between the S-band and X-band downlinks provided interplanetary media calibrations for the S-band Doppler. Analogous calibrations were considered for Cassini, which is tracked at X band and has an additional K*a*-band downlink. However, X-band Doppler is much less sensitive to transmission media effects than S band, and the K*a*-band downlink is not normally transmitted owing to operational considerations. Consequently, the Cassini project elected not to calibrate for interplanetary media. We, however, did use a solar plasma model to calibrate for both Voyager (when S–X calibrations are unavailble) and Cassini range delays.

The Voyager imaging observations are the sample and line locations of images of the satellites and background reference stars as seen with the Voyager Vidicon system. The imaging data arcs begin at the same time as the respective tracking data arcs and end on 1980 November 12 for Voyager 1 (just prior to encounter) and on 1981 August 31 for Voyager 2 (5 days after encounter). The Cassini imaging observations, like those from Voyager, are the sample and line locations of images of the satellites and background reference stars. However, the Cassini cameras have charge-coupled device (CCD) detectors rather than the Vidicon system of Voyager. During mission operations, the Cassini Navigation team used observations of only eight of the main satellites and Phoebe. Titan was excluded from the imaging data because its atmosphere corrupted the image reduction process. We extended the observation set to include imaging of the main satellites, the Lagrangians, Methone, and Phoebe provided by the Cassini Imaging Science team. The Cassini imaging began on 2004 February 6 and ended on 2017 March 31.

Our Earth-based satellite astrometry data arc begins with the visual micrometer measurements made during the years 1874–1947 and extends through the CCD observations of the main satellites made at the Table Mountain Observatory in 2017 July and those of Phoebe made at Purple Mountain Observatory in 2019 July. There is a gap in the astrometry between 1947 and 1966. (The gap is generally attributed to lack of interest in the astronomical community for solar system observing. The advent of the space age apparently revived that interest.) The HST observations cover the period from the Saturn ring plane crossing in 1995 to January of 2005. The mutual event observations cover the periods 1979–1980, 1995–1996, and 2008–2009. The transits span 1985–2007. The astrometry is in the form of satellite-to-satellite relative positions, satellite-to-planet relative positions, and absolute satellite positions. The latter include the transits and satellite stellar occultations. The mutual event eclipses and occultations were reported in the form of relative positions.

We retained all of the data previously processed in Jacobson (2004) and Jacobson et al. (2006a). Neither of those analyses fit data prior to 1938, but for this work we processed all of the main satellite observations contained in the catalog of Strugnell & Taylor (1990) and evaluated and validated by Harper & Taylor (1994). We extended the Phoebe observation set back to its discovery; Jacobson (1998) previously processed that earlier data. We added the following main satellite data sets:

1. Observatoire Royal de Belgique photographic astrometry in 1977 (Debehogne 1979).
2. Main Astronomical Observatory of Ukrainian Academie of Science photographic astrometry in 1980 (Izhakevich 1991).
3. Tokyo-Mitaka photographic astrometry from 1970 to 1972 (Hatanaka 1995).
4. Golosseevo-Kiev Observatory photographic astrometry from 1963 to 1984 (Filippov 2001; Izhakevich 2001).
5. Yunnan Observatory CCD astrometry from 2002 to 2006 (Peng et al. 2008).
6. Pulkovo Observatory CCD astrometry from 2002 to 2009 (Khrutskaya et al. 2009; Kisseleva 2009; Grosheva et al. 2011).
7. Mutual occultations and eclipses in 2009 (Arlot et al. 2012).
8. CCD meridian instrument astrometry from Bordeaux from 2001 to 2007 (Arlot et al. 2008).
9. Flagstaff Astrometric Scanning Transit Telescope (FASTT) astrometry taken from 2006 to 2016 (Monet 2005–2007; Harris 2007–2016).
10. Table Mountain Observatory CCD astrometry from 2009 to 2017 (Owen 2018).
11. Stellar occultations in 1974, 2002, and 2014 (Herald et al. 2020).

Additional Phoebe data sets were also included:

1. CCD astrometry from Haute Provence, European Southern Observatory, and Itajuba Observatory from 1996 to 2014 (Gomes-Júnior et al. 2015).
2. CCD astrometry from Yunnan Observatory from 2003 to 2005 (Peng & Zhang 2006) and from 2011 to 2014 (Peng et al. 2015).
3. CCD astrometry from Sheshan Station and Peking Observatory from 2003 to 2008 (Qiao et al. 2006, 2011).
4. Flagstaff Astrometric Scanning Transit Telescope (FASTT) astrometry taken from 2003 to 2005 (Stone 2001–2005).
5. Table Mountain Observatory CCD astrometry from 2004 to 2009 (Owen 2018).
6. CCD astrometry from many observatories collected by the Minor Planet Center from 2004 to 2019 (MPC 2000–2019).

The Natural Satellites Astrometric Database (NSDB; Arlot & Emelyanov 2009) contains most of the astrometry.

We corrected the Earth-based photographic and CCD astrometry for the defect of illumination, the offset between the satellite's center of body and center of light, based on the relations from Lindegren (1977): $\Delta\alpha = C\ R \sin(i/2) \sin Q \sec\delta$ and $\Delta\delta = C\ R \sin(i/2) \cos Q$, where $\Delta\alpha$ and $\Delta\delta$ are the corrections in R.A. and decl., C is a constant determined from scattering theory (we adopted $C = 0.75$ as suggested by Lindegren), R is the radius of the object, Q is the position angle of the greatest defect of illumination, i is the phase angle, and δ is the declination. No corrections were applied to the FASTT data, as they had already been corrected by the observers. Nor did we correct the micrometer data, as we expect the phase effects to be absorbed in our corrections for the observer's "personal equation" (discussed in the following section).

The Saturn ring occultation measurements are in the form of the occultation times and radii of the occulting rings. Simpson et al. (1983) first found the orientation of Saturn's pole by analyzing the Voyager occultations. Nicholson et al. (1990) later reexamined the data and improved the pole direction. The 1989 stellar occultation of the rings led to a pole estimate by Hubbard et al. (1993). French et al. (1993) followed up by combining that occultation with those from Voyager. Elliot et al. (1993) obtained his pole direction from the 1989 occultation in combination with the 1991 stellar occultation observed with HST. French et al. (2017) combined all of the previous occultations with the 1995 HST stellar occultation and those observed with the Cassini spacecraft through the end of 2013. We restricted our data set to 10,600 occultations of 67 strictly circular rings extracted from French et al. (2017) and supplemented by the occultations acquired by Cassini after 2013 (French 2018, private communication).

The Saturn ring plane position angles are visually measured position angles of the rings (Barnard 1891a, 1891b, 1910, 1927). The ring plane crossing times are the times at which the ring plane appeared edge-on as seen from Earth: 1907 October (Innes 1908), 1908 January (Barnard 1908b; no specific time was given, but Barnard states that the crossing probably occurred between 1908 January 5 12:00 GMT and 1908 January 7 11:15 GMT and that the ring was visible on January 7; we arbitrarily set the time to 1908 January 7 08:15 GMT), 1996 December (Kiladze 1969), 1996 December (Dollfus 1979), 1995 May (Bosh et al. 1997), and 1995 August (Nicholson et al. 1996; we used the midpoint of the east and west ansa crossing times).

4. Solution Method and Results

4.1. Parameter Estimation and Data Weights

We determined the orbits of the satellites, the gravitational parameters, and the Saturn pole orientation from a weighted least-squares fit to the observational data with a square root information filter (Lawson & Hanson 1974; Bierman 1977). Separate square root information (SRI) arrays were generated for each observation set; the data from each spacecraft trajectory and each Cassini trajectory segment (the trajectory was subdivided into 149 segments containing one or more orbits) were treated as separate data sets. We combined the separate SRI arrays to produce a composite SRI array for the estimated parameters:

1. Satellite epoch states.
2. Saturn's system and satellite *GM*s.
3. Gravitational harmonics of Saturn.
4. The k_2 Love number of Saturn.
5. Satellite-dependent time lags for the tides raised on Saturn.
6. Gravitational harmonics of Enceladus, Dione, Rhea, and Titan.
7. Saturn's pole orientation and axial moment of inertia.
8. Occulting ring radii.
9. Corrections for the Cassini RSS ring occultations needed to remove systematic biases introduced during the data reduction process (French et al. 2017).
10. Satellite-dependent phase angle biases in the Cassini optical data; these biases account for the error in determining the center of the image of a partially illuminated object.
11. Camera pointing angles; the inertial pointing for each picture is adjusted based on the background stars appearing in the picture.
12. Camera sample and line biases; these are effectively a recalibration of the center of the camera frame.
13. Onboard oscillator frequency biases and drift rates for the one-way noncoherent Doppler.
14. Ionosphere corrections for Pioneer 11 Doppler (troposphere but not ionosphere calibrations are available for Pioneer 11).
15. Tracking station-dependent range biases; these correct the errors in the range calibrations and offset any remaining Saturn ephemeris errors.
16. Observer-dependent position angle and separation biases in the visual micrometer data; these account for the systematic errors known as the observer's "personal equation."
17. Scale and orientation corrections for the CCD detector in some of the Earth-based astrometry; in the reduction of their data, several observers (Vass 1997; Veiga & Vieira Martins 1999; Vienne et al. 2001; Peng et al. 2002, 2008; Veiga et al. 2003) calibrated the scale and orientation of their CCD detector following a procedure that relies on positions of the satellites predicted from preexisting ephemerides; our corrections minimize the calibration errors introduced by errors in those ephemerides.
18. Telescope pointing direction for those CCD observations provided in their raw sample and line format (Harper et al. 1997, 1999; Qiao et al. 1999, 2004).
19. Opposition-dependent R.A. and decl. biases in the absolute photographic and CCD astrometry to mitigate possible star catalog errors and remaining Saturn ephemeris errors.
20. Station-dependent timing offsets for the Earth-based and HST stellar ring occultations.
21. Timing corrections for the Cassini ring stellar occultations.
22. Occulted star proper motions for the Earth-based and HST stellar ring occultations.

We grouped the astrometric data (Earth-based and HST) according to type, observatory, and the observing period in which they were acquired. We selected data weights for each group through an iterative process to be consistent with the rms of the residuals (the differences between the actual observations and their values predicted by our model) of that group.

We set separate Doppler data weights for each DSN pass to correspond to an accuracy consistent with the residuals for that pass. The weights were determined by applying a scale factor to the rms of the residuals to account for the fact that the Doppler noise is not a white-noise process (Folkner 1994). The scale factor is $0.470(86400/\tau)^{1/3}$, where τ is the Doppler sample interval in seconds. However, this factor produces a weight that is too conservative for the satellite close encounter data. For those data we applied a scale factor of 1.1 when the troposphere dominated the data noise and adopted the Doppler whitening algorithm (Mackenzie & Folkner 2006) when the solar plasma dominated the data noise.

The range data were also weighted on a pass-by-pass basis with weights derived from the rms of the data residuals scaled by the square root of the number of points in the pass. The scaling suppresses range rate information inferred from the

Table 3
Imaging Scale Factors

Satellite	Scale	Satellite	Scale	Satellite	Scale
Mimas	0.020	Titan	0.010	Telesto	0.500
Enceladus	0.015	Hyperion	0.250	Calypso	0.500
Tethys	0.010	Iapetus	0.020	Polydeuces	0.300
Dione	0.010	Phoebe	0.100	Methone	0.500
Rhea	0.010	Helene	0.250		

change in the range during the pass and allows the Doppler data to be the primary source of that information.

For the spacecraft imaging we assigned an accuracy of 0.25 pixels to the stars for Voyager and 0.1–0.2 pixels for Cassini (depending on the data reduction). For the satellites we computed the accuracy from the expression $\sigma^2 = \sigma_{\text{base}}^2 + (C\ d_a)^2$, where σ is the assigned accuracy, σ_{base} is a base accuracy of 0.5 pixels, d_a is the satellite's apparent diameter, and C is an empirical scale factor given in Table 3. The overall accuracy of the imaging data was also influenced by the accuracy of the camera pointing for each picture as estimated independently during the data processing. The ultimate quality of the pointing for a picture was dictated by the number and distribution of the background stars in the picture.

The ring occultation observables are the radial distances of various ring features at the recorded occultation times. Based on the residual rms, we set the measured distance accuracies at between 1.0 and 2.0 km depending on the feature. The weights for the timing of the ring plane crossings were set according to the accuracies suggested by the observers. Similarly, following the suggestion of the observer, the accuracies assumed for the ring plane position angles were 0.″15–0.″25 in 1891 and 1892, 0.″20 in 1906 and 1907, and 0.″30 in 1920 and 1921.

4.2. System and Satellite GMs and Densities

Table 4 gives our current *GM* results, along with those from our previous published investigations. With the exception of Helene, we have determined all *GM*s to a fraction of 1%. As stated earlier, we were unable to estimate the ring *GM*s; however, they are included in our system *GM* (see Table 2). The entries in the table show that there has been little change in the system and main satellite *GM*s since the first publication based on the early Cassini data (Jacobson et al. 2006a). The uncertainties on them, however, have improved considerably.

The Cassini Doppler tracking acquired during the Saturn periapsis passages and the Enceladus, Rhea, Titan, Hyperion, Iapetus, and Phoebe flybys is the primary source of information on their *GM*s. The Pioneer and Voyager data provide additional information for Saturn, Rhea, Titan, and Iapetus.

The mean motions of Mimas and Tethys are in a near 4:2 commensurability, resulting in a mean longitude libration with about a 72 yr period. There is a 2:1 mean motion commensurability between Enceladus and Dione that causes a ∼11 yr period libration and a ∼3.8 yr period circulation. These commensurabilities amplify the dynamical interaction of the satellites, and a number of investigators found their *GM*s from astrometric observations of their motions. But the Lagrangian satellites provide a more accurate and independent source of information on the Tethys and Dione *GM*s. Helene oscillates about the leading triangular libration point L_4 of Dione with a period of about 768 days, and Polydeuces oscillates about the trailing L_5 point with a period of about 792 days. Telesto and Calypso oscillate about the Tethys leading and trailing libration points, respectively, with periods of roughly 696 days. Astrometric and spacecraft imaging observations of the librations lead to precise estimates for the Dione and Tethys *GM*s. The contribution from Cassini Doppler tracking data during the Tethys and Dione flybys is negligible. On the other hand, the tracking from the flybys of Enceladus enabled its *GM* determination to be several orders of magnitude more accurate than one made from the resonance with Dione. Mimas is a strong perturber of the orbit of the small satellite Methone, and observations of that perturbation determine the Mimas *GM* far better than the Mimas perturbations on Tethys.

Theoretically, it should be possible to obtain the Lagrangian satellite *GM*s from their perturbations on Tethys and Dione. However, as these satellites are quite small, those perturbations are nearly unobservable. Surprisingly, we find that the cumulative effect of Helene on Dione appears to noticeably affect the Cassini tracking data during the Dione flybys. Consequently, we are able to extract an estimate of Helene's *GM*.

The satellite masses and densities derived from their *GM*s appear in Table 5; the masses are based on $G = (6.67430 \pm 0.00015) \times 10^{-23}$ km^3 g^{-1} s^{-2}. Thomas (2010) measured the radii of the main satellites and Phoebe. Helene's radius is from Thomas et al. (2013), and that of Titan is from Corlies et al. (2017). Except for Hyperion and Helene, the bulk densities are consistent with mixtures of ice and rock. The low densities of Hyperion and Helene suggest the presence of a significant amount of porosity. It may be that Helene is simply a loose pile of rubble that has accumulated at the Lagrange point. It is worth noting that our estimated Helene density is significantly less than the theoretical prediction of Thomas et al. (2018) based on topographic features. However, we found that if we used either a massless Helene or a Helene *GM* based on an assumed density of 0.5 g cm^{-3} in our orbit integration, our fit to the Dione flyby data was degraded. It is likely, therefore, that our *GM* estimate is realistic.

4.3. Saturn Gravity Field

Besides the Pioneer 11 and Voyager flybys, there were 15 Cassini Saturn periapsis passages for which there is continuous or near-continuous tracking prior to the five dedicated gravity science periapses[1] during the Cassini Grand Finale. It is interesting that until the Grand Finale the Pioneer 11 periapsis was the lowest.

Table 6 contains the values that have been determined for the zonal harmonics of Saturn from the fit to our complete data set. Also in the table is our estimate of Saturn's Love number. In the results appearing in the table, Null et al. (1981) fit only Pioneer 11 data, both Campbell & Anderson (1989) and Jacobson (2004) combined the data from Pioneer 11 and Voyager, and Jacobson et al. (2006a) used Cassini data, but only those acquired prior to 2006 July. The Cassini Gravity Science Team (Iess et al. 2019) obtained their final results from short arc fits to only the five Grand Finale gravity passes. None of the previous analyses accounted for the tide raised on Saturn by the satellites. Our harmonics are in fair agreement with Iess et al., and our values for J_2, J_4, and J_6 are in statistical agreement with those we published in 2006.

[1] Periapsis 275 was a planned sixth gravity science periapsis, but the close flyby data were lost.

Table 4
Saturnian System *GM*s ($km^3\ s^{-2}$)

Parameter	Jacobson (2004)	Jacobson et al. (2006a)	Current
GM_{sys}	37940672. ± 59.	37940585.23 ± 1.11	37940584.920 ± 0.178
GM_{Saturn}	37931284. ± 57.	37931207.68 ± 1.11	37931206.234 ± 0.726
GM_{Mimas}	2.55 ± 0.05	2.5023 ± 0.0020	2.50349 ± 0.00042
$GM_{Enceladus}$	6.95 ± 1.5	7.2096 ± 0.0067	7.21037 ± 0.00027
GM_{Tethys}	41.21 ± 0.08	41.2097 ± 0.0063	41.21353 ± 0.00094
GM_{Dione}	73.12 ± 0.02	73.1127 ± 0.0025	73.11607 ± 0.00016
GM_{Rhea}	155.59 ± 4.9	153.9416 ± 0.0049	153.94175 ± 0.00123
GM_{Titan}	8978.08 ± 0.8	8978.1356 ± 0.0039	8978.13710 ± 0.00074
$GM_{Hyperion}$	0.72 ± 0.35	0.3727 ± 0.0045	0.37049 ± 0.00015
$GM_{Iapetus}$	129.66 ± 17.	120.5117 ± 0.0173	120.51511 ± 0.00727
GM_{Phoebe}	0.48 ± 0.23	0.5534 ± 0.0006	0.55479 ± 0.00325
GM_{Helene}			0.00048 ± 0.00005

Note. GM_{sys} includes the rings; quoted uncertainties are 3σ.

Table 5
Satellite Physical Properties

Body	Radius (km)	Mass (10^{20}g)	Density (g cm^{-3})
Mimas	198.20 ± 0.40	375.094 ± 0.023	1.1501 ± 0.0070
Enceladus	252.10 ± 0.20	1080.318 ± 0.028	1.6097 ± 0.0038
Tethys	531.10 ± 0.60	6174.959 ± 0.146	0.9840 ± 0.0033
Dione	561.40 ± 0.40	10,954.868 ± 0.246	1.4781 ± 0.0032
Rhea	763.50 ± 0.60	23,064.854 ± 0.522	1.2372 ± 0.0029
Titan	2574.76 ± 0.02	1,345,180.354 ± 30.232	1.8814 ± 0.0001
Hyperion	135.00 ± 4.00	55.510 ± 0.007	0.5386 ± 0.0479
Iapetus	734.30 ± 2.80	18,056.591 ± 0.544	1.0887 ± 0.0125
Phoebe	106.50 ± 0.70	83.123 ± 0.162	1.6428 ± 0.0326
Helene	18.00 ± 0.40	0.071 ± 0.002	0.2926 ± 0.0217

Note. Quoted uncertainties are 1σ.

Table 6
Saturn Gravity Fields

Parameter	Null (1981)	Campbell (1989)	Jacobson (2004)
$J_2 \times 10^{-6}$	16,299.0 ± 18.0	16,298.0 ± 10.0	16,292.0 ± 7.0
$J_4 \times 10^{-6}$	−916.0 ± 38.0	−915.0 ± 40.0	−931.0 ± 31.0
$J_6 \times 10^{-6}$	81.0	103.0 ± 50.0	91.0 ± 31.0
$J_8 \times 10^{-6}$		−10.0	−10.0
Parameter	**Jacobson et al. (2006a)**	**Iess et al. (2019)**	**Current**
$J_2 \times 10^{-6}$	16,290.71 ± 0.27	16,290.573 ± 0.028	16,290.615 ± 0.025
$J_3 \times 10^{-6}$		0.059 ± 0.023	0.095 ± 0.040
$J_4 \times 10^{-6}$	−935.83 ± 2.77	−935.314 ± 0.037	−935.119 ± 0.093
$J_5 \times 10^{-6}$		−0.224 ± 0.054	−0.060 ± 0.137
$J_6 \times 10^{-6}$	86.14 ± 9.64	86.340 ± 0.087	86.764 ± 0.162
$J_7 \times 10^{-6}$		0.108 ± 0.122	0.481 ± 0.148
$J_8 \times 10^{-6}$	−10.	−14.624 ± 0.205	−13.931 ± 0.217
$J_9 \times 10^{-6}$		0.369 ± 0.260	0.892 ± 0.136
$J_{10} \times 10^{-6}$		4.672 ± 0.420	5.426 ± 0.208
$J_{11} \times 10^{-6}$		−0.317 ± 0.458	0.147 ± 0.186
$J_{12} \times 10^{-6}$		−0.997 ± 0.672	−0.537 ± 0.180
k_2		0.382 ± 0.025	

Note. Reference radius for the gravitational harmonics: 60,330 km. The quoted uncertainties are the formal 3σ uncertainties.

Saturn's Love number k_2 is found primarily from the tidal effects on the Lagrangian satellites due to tides raised on Saturn by the main satellites. This result was first reported by Lainey et al. (2017). Our value agrees with their published value of 0.390 ± 0.024 but differs from the theoretically predicted value of 0.413 (Wahl et al. 2017) by nearly 5σ.

Table 7
Satellite Quadrupole Moments $\times 10^6$

deg n	ord m	Mimas[1] C_{nm}	Enceladus[2] C_{nm}	Tethys[3] C_{nm}	Dione[4] C_{nm}	Rhea[5] C_{nm}	Titan[6] C_{nm}	Iapetus[7] C_{nm}
2	0	−35,511	−5533	−8724	−1456	−8929	−32.44	−17,600
2	2	8385	1540	3062	356	239	10.37	0

Note. Reference radii = 207.8[1], 256.6[2], 538.4[3], 563.4[4], 765[5], 2575[6], 745.7[7].

4.4. Satellite Gravity Quadrupoles

Our dynamical model did not treat the largest satellites as point masses. Instead, we represented their extended body gravity fields by the C_{20} and C_{22} moments of their gravity quadrupole. Table 7 contains the values adjusted to the reference radii that are equal to the satellites' subplanetary equatorial radii (Archinal et al. 2018).

In the Cassini tour there were no flybys of Mimas and Tethys sufficiently close to provide data for the determination of their gravitational harmonics. In the absence of direct measurement, we computed our C_{20}, C_{22} assuming uniform density coupled with the shape models of Nimmo and Bills (2011).

There was one Iapetus encounter in the Cassini tour, but there was no tracking during the flyby. However, the Cassini Navigation Team found that the spacecraft trajectory modeling was improved if the effect of an Iapetus C_{20} was included (Antreasian et al. 2008). They adopted the value of $C_{20} = -18{,}300.0 \times 10^{-6}$ from a uniform-density ellipsoid of revolution with polar and equatorial radii of 712.4 and 747.4 km, respectively. Our value is based on the IAU radii of 712.1 and 745.7 km.

We determined the remaining quadrupole moments from the effect of the satellites' gravity on the Cassini spacecraft. Iess et al. (2014) estimated the Enceladus gravity field from data acquired during three flybys dedicated to gravity field determination. Our quadrupole is in statistical agreement with Iess et al. at the 1σ level. The Cassini Radio Science team published a gravity field for Dione based on tracking from three flybys (Zannoni et al. 2020). As with Enceladus, our quadrupole agrees with theirs at about the 1σ level. Tortora et al. (2016) reported the Rhea gravity field obtained from two Cassini flybys. We are in good agreement with their C_{22} harmonic but disagree by nearly 2.5σ with their C_{20}. Our analysis found that the gravity field determination is significantly dependent on the Rhea ephemeris. The Cassini tour contained 10 flybys of Titan that were dedicated to acquiring data for the determination of its gravity field. Our C_{20} and C_{22} statistically match the results found by the Cassini Radio Science team (Durante et al. 2019).

4.5. Saturn Pole and Moment of Inertia

As described in the Appendix, our model for the motion of the pole of Saturn is the rotation of a rigid body. We numerically integrated the rotational equations over the 400 yr period from 1800 to 2200. To compute the torques, we took the masses of the Sun and Jupiter from Table 1, the satellite masses from Table 4, and Saturn's zonal harmonics from Table 6. The Saturn spin rate, $818.138776369\,^{+1.70}_{-2.40}$ deg day^{-1}, is from Mankovich et al. (2019).

We fit the following Fourier series to the numerically integrated pole orientation angles (α is ICRF R.A., δ is decl., W is prime meridian):

$$\begin{aligned}\alpha = {} & 40^\circ.594872 - 0^\circ.0554684758\,T + 0^\circ.031424\sin S01 \\ & + 0^\circ.000371\sin S03 + 0^\circ.000093\sin S04 \\ & + 0^\circ.000508\sin S06 + 0^\circ.000064\sin S08 \\ & - 0^\circ.000257\sin S09 - 0^\circ.000018\sin S10\end{aligned} \tag{1}$$

$$\begin{aligned}\delta = {} & 83^\circ.534351 - 0^\circ.0063345961\,T + 0^\circ.003627\cos S01 \\ & - 0^\circ.000019\cos S02 + 0^\circ.000042\cos S03 \\ & - 0^\circ.000009\cos S05 - 0^\circ.000057\cos S06 \\ & + 0^\circ.000005\cos S07 - 0^\circ.000007\cos S08 \\ & - 0^\circ.000029\cos S09\end{aligned} \tag{2}$$

$$\begin{aligned}W = {} & 38^\circ.814623 + 818^\circ.1387763691\,d - 0^\circ.031224\sin S01 \\ & - 0^\circ.000368\sin S03 - 0^\circ.000093\sin S04 \\ & - 0^\circ.000505\sin S06 - 0^\circ.000063\sin S08 \\ & + 0^\circ.000255\sin S09 + 0^\circ.000018\sin S10,\end{aligned} \tag{3}$$

with

$$\begin{aligned} S01 &= 335^\circ.808773 + 51^\circ.9103094\,T, \\ S02 &= 348^\circ.007386 + 94^\circ.9443923\,T \\ S03 &= 9^\circ.358404 + 1004^\circ.8552318\,T, \\ S04 &= 129^\circ.758867 + 1222^\circ.9801079\,T \\ S05 &= 219^\circ.758867 + 1222^\circ.9801079\,T, \\ S06 &= 159^\circ.835383 + 2445^\circ.2110530\,T \\ S07 &= 249^\circ.835383 + 2445^\circ.2110530\,T, \\ S08 &= 117^\circ.222690 + 3667^\circ.7456916\,T \\ S09 &= 280^\circ.168047 + 7226^\circ.4296474\,T, \\ S10 &= 7^\circ.050371 + 36506^\circ.7196194\,T \end{aligned}$$

T = Julian centuries from epoch J2000, and d = days from epoch J2000. The trigonometric arguments in the series are a consequence of the orbit precessions of Titan (S01, S02), Rhea (S03), Tethys (S09), and Mimas (S10) and the orbital motion of Saturn (S04, S05, S06, S07, S08). Because of their small inclinations, the orbit precessions of Enceladus and Dione do not contribute significant periodic effects. The long-period precession of Iapetus is absorbed by the linear terms that also account for the Jupiter and Sun torques. At epoch J2000, $W = 38^\circ.90$, in agreement with the IAU definition of the prime meridian (Archinal et al. 2018). The series is truncated at the 4 microdegree level.

As part of our procedure for fitting the observational data, we estimate the R.A. and decl. of the pole, i.e., the constant terms in the pole series, and Saturn's axial moment of inertia (MOI). Our values for those parameters appear in Table 8. The quoted rotation rate uncertainty has a negligible contribution to that of the MOI. The table also contains the pole parameters for a case in which the ring occultations were omitted. The two sets of

Table 8
Saturn Pole Parameters

Rt. Ascen.	Decl.	MOI[a]	Source
$40.^{\circ}594872 \pm 0.^{\circ}000156$	$83.^{\circ}534351 \pm 0.^{\circ}000029$	0.2258 ± 0.0025	all data
$40.^{\circ}594761 \pm 0.^{\circ}000171$	$83.^{\circ}534380 \pm 0.^{\circ}000032$	0.2288 ± 0.0034	no occultations

Note.
[a] Reference radius = 60,330 km; quoted uncertainties are 1σ.

Table 9
Saturn Moment of Inertia[a]

Value	Source	Value	Source
0.2200	Fortney & Hubbard (2003)	0.2219	Movshovitz et al. (2020)
0.2228	Anderson & Schubert (2007)	0.2193	Radau–Darwin (Murray & Dermott 1999)
0.2197	Hubbard et al. (2009)	0.2296	Radau–Darwin (Yoder 1995)
0.2175	Helled (2011)	0.2263 ± 0.0101	current

Note.
[a] Reference radius = 60,268 km; quoted uncertainty is 3σ.

Table 10
Tidal Dissipation

Satellite	Lag Time (s)	Q_{Si}	$k_2/Q_{Si} \times 10^4$
Mimas	3.719 ± 1.259	1526 ± 517	2.510 ± 0.853
Enceladus	1.421 ± 0.592	3136 ± 1317	1.221 ± 0.514
Tethys	0.258 ± 0.210	$15{,}274 \pm 12{,}399$	0.251 ± 0.204
Dione	0.648 ± 0.126	5567 ± 1117	0.688 ± 0.139
Rhea	8.299 ± 1.100	404 ± 54	9.483 ± 1.274
Titan	2.542 ± 0.248	1224 ± 119	3.129 ± 0.313

Note. Saturn Love number = 0.3830 ± 0.0084. Quoted uncertainties are 1σ.

Table 11
Tidal Dissipation—Earth-based Astrometry and Cassini Imaging Data

Satellite	Lag Time (s)	Q_{Si}	$k_2/Q_{Si} \times 10^4$
Mimas	2.817 ± 1.727	2015 ± 1236	1.901 ± 1.166
Enceladus	2.660 ± 0.762	1676 ± 480	2.286 ± 0.657
Tethys	0.428 ± 0.236	9225 ± 5084	0.415 ± 0.229
Dione	0.548 ± 0.735	6583 ± 8833	0.582 ± 0.781
Rhea	12.232 ± 3.092	274 ± 69	13.777 ± 3.546
Titan	34.166 ± 37.800	91 ± 101	42.060 ± 46.542

Note. Quoted uncertainties are 1σ.

parameters are statistically in agreement with some slight improvement provided by the occultations.

Table 9 contains our MOI, together with several predictions based on various models of Saturn's interior, as well as values calculated with two different versions of the Radau–Darwin relation. The MOI value in Table 8 is associated with the reference radius of Saturn's gravitational harmonics, 60,330 km. For Table 9 we adjusted it to Saturn's equatorial radius, 60,268 km, to be consistent with the radius used in the published predictions. Our value lies between the two Radau–Darwin values and is larger than all of the theoretical predictions but is within 3σ of all of those predictions.

The comparison of the various MOI values should be exercised with some caution. Our value is obtained from Saturn's angular momentum assuming that Saturn is a rigid body rotating at the rate from Mankovich et al. (2019) with torques applied by the satellites, Jupiter, and the Sun. Moreover, we are assuming that the Saturn pole needed to orient the Saturn gravity field is aligned with that angular momentum vector. The other values follow from various theoretical models for Saturn's interior and are unrelated to Saturn's angular momentum. In general, the theoretical models obtain their MOI from the postulated interior density distribution in the model.

4.6. Tidal Dissipation

Our force model includes the effects of the tides raised on Saturn by Mimas, Enceladus, Tethys, Dione, Rhea, and Titan and the tide raised on Enceladus by Saturn. We include the latter because it is presumed to be the source of the heat being dissipated in Enceladus (Nimmo et al. 2018) and contributes to the overall tidal acceleration of Enceladus. In the analysis we determined not only Saturn's k_2 but also Saturn's satellite-dependent time lags, Δt_{Si}, in the tide force model. The tidal time lag associated with satellite i is related to the corresponding tidal quality factor, Q_{Si}, through the lag angle δ_{Si} (Efroimsky & Lainey 2007),

$$\delta_{Si} = \frac{\Delta t_{Si}}{r_i} |\dot{W}\,(\boldsymbol{r}_i \times \hat{\boldsymbol{k}}) + \dot{\boldsymbol{r}}_i|,$$
$$Q_{Si}^{-1} = \tan 2\delta_{Si},$$

where $\dot{W}$ is Saturn's rotation rate, $\hat{\boldsymbol{k}}$ is Saturn's pole, and $\boldsymbol{r}_i$, $\dot{\boldsymbol{r}}_i$ are the satellite's Saturn-relative position and velocity.

To account for the tide raised on Enceladus, we set its $k_2/Q = 0.0065$, a value that falls solidly within the range of theoretical values quoted by Nimmo et al. (2018) and corresponds to a heat flow of 10.3 GW. We found that the dissipation in Enceladus was crucial to our analysis. If we omitted it, we obtained a nonphysical Enceladus-dependent dissipation in Saturn. Varying the Enceladus k_2/Q (within the range quoted by Nimmo et al.) did not significantly alter the total Enceladus tidal acceleration, as the dissipation in Saturn simply adjusted to compensate for the change. Clearly, Enceladus is affected by tides, but the data alone are

Table 12
Planetocentric Orbital Elements Referred to the Local Laplace Planes at Epoch 2000 January 1.5 (TDB)

Satellite	a (km)	e	i (deg)	Period (days)	P_ω (yr)	P_Ω (yr)	ϵ (deg)
Mimas	186,000.	0.020	1.6	0.942422	0.493	0.986	0.0
Enceladus	238,400.	0.005	0.0	1.370218	2.916	0.000	0.0
Tethys	295,000.	0.001	1.1	1.887802	0.005	4.982	0.0
Dione	377,700.	0.002	0.0	2.736916	11.698	0.000	0.0
Rhea	527,200.	0.001	0.3	4.517503	33.939	35.775	0.0
Titan	1,221,900.	0.029	0.3	15.945448	346.680	687.370	0.6
Hyperion	1,481,500.	0.105	0.6	21.276658	20.843	257.625	0.1
Iapetus	3,561,700.	0.028	7.6	79.331002	1662.900	3130.302	14.8
Phoebe[a]	12,929,400.	0.164	175.2	550.303910	468.321	741.483	26.7
Helene	377,600.	0.007	0.2	2.736916	5.825	11.707	0.0
Telesto	295,000.	0.001	1.2	1.887802	0.005	4.982	0.0
Calypso	295,000.	0.001	1.5	1.887803	0.005	4.983	0.0
Methone	194,700.	0.002	0.0	1.009549	0.003	0.000	0.0
Polydeuces	377,600.	0.019	0.2	2.736916	5.810	11.692	0.0

Note.
[a] Saturnian system barycentric elements.

Table 13
Satellite Orbit 1σ Uncertainties

Satellite	Radial	Downtrack	Normal	Satellite	Radial	Downtrack	Normal	Year
Mimas	1.2 km	10.7 km	1.6 km	Iapetus	4.0 km	14.1 km	8.0 km	2018
	2.2 km	65.1 km	2.1 km		4.0 km	24.2 km	8.0 km	2033
Enceladus	35 m	4.8 km	457 m	Phoebe	17.4 km	81.3 km	13.0 km	2018
	126 m	9.2 km	569 m		22.5 km	131.8 km	15.1 km	2033
Tethys	1.4 km	4.1 km	1.8 km	Helene	1.1 km	4.3 km	2.0 km	2018
	1.4 km	9.6 km	1.8 km		1.1 km	7.5 km	2.1 km	2033
Dione	1.0 km	3.4 km	2.3 km	Polydeuces	856 m	3.8 km	1.5 km	2018
	1.0 km	6.8 km	2.5 km		893 m	9.9 km	1.6 km	2033
Rhea	2.1 km	7.9 km	3.2 km	Telesto	1.5 km	5.6 km	2.5 km	2018
	2.1 km	15.0 km	3.4 km		1.5 km	10.9 km	2.6 km	2033
Titan	250 m	1.3 km	1.2 km	Calypso	1.4 km	6.6 km	2.5 km	2018
	261 m	1.8 km	1.2 km		1.4 km	13.4 km	2.5 km	2033
Hyperion	8.5 km	46.4 km	11.8 km	Methone	1.1 km	12.4 km	3.5 km	2018
	17.1 km	97.1 km	11.8 km		1.1 km	62.5 km	3.5 km	2033

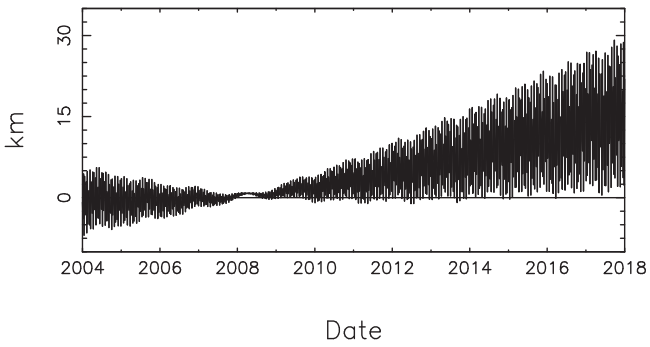

Figure 1. Mimas in-orbit differences from SAT427.

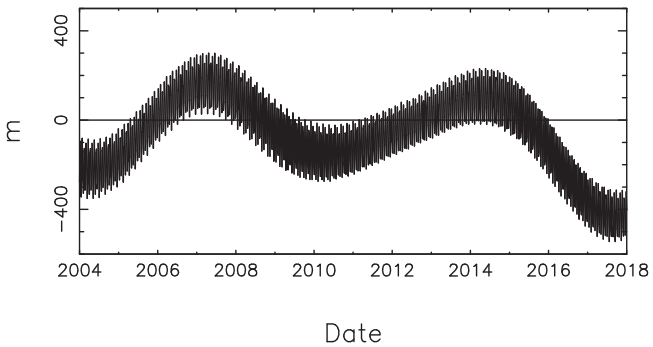

Figure 2. Enceladus in-orbit differences from SAT427.

insufficient to distribute the effect between the satellite and planet contributions. As the objective of our work is to develop ephemerides of the satellites, not to investigate tidal effects, we have simply retained our selected Enceladus k_2/Q, as it produces an orbit that is consistent with a high-quality fit to all of the Cassini Enceladus flyby data. Table 10 contains our tidal parameters.

As a test we also developed an ephemeris using all of the data except the Voyager 1 and Cassini tracking data but retaining the gravitational parameters and Saturn pole. The tidal parameters associated with this ephemeris appear in Table 11. For all satellites the uncertainties grow, and there are significant changes in the tidal parameters, particularly in those of Rhea and Titan. In fact, the Titan Q_{Si} becomes indeterminate; its

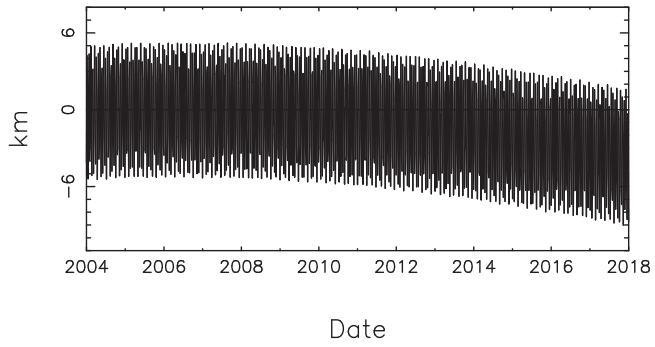

Figure 3. Tethys in-orbit differences from SAT427.

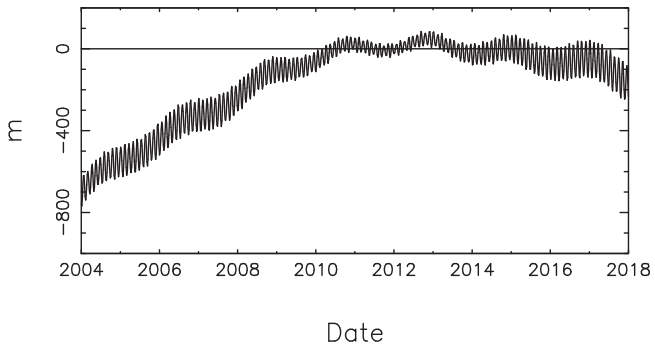

Figure 4. Dione in-orbit differences from SAT427.

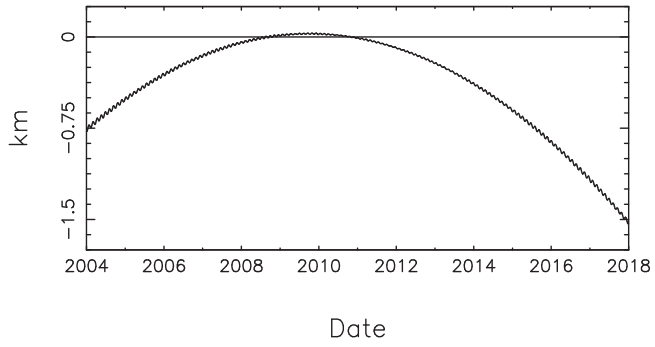

Figure 5. Rhea in-orbit differences from SAT427.

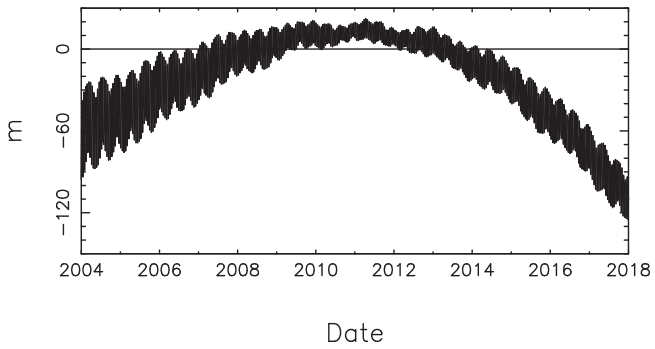

Figure 6. Titan in-orbit differences from SAT427.

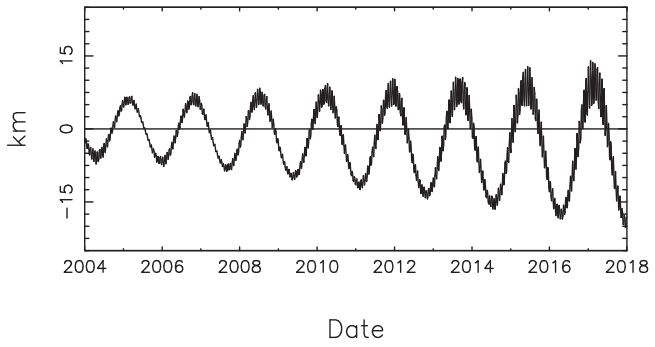

Figure 7. Hyperion in-orbit differences from SAT427.

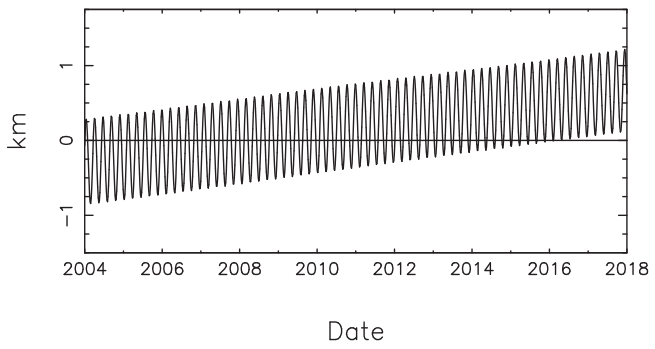

Figure 8. Iapetus in-orbit differences from SAT427.

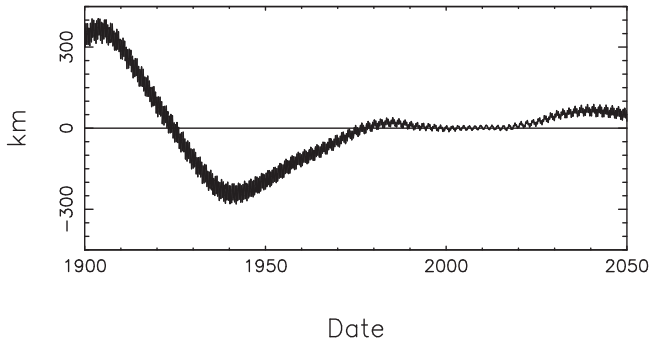

Figure 9. Mimas in-orbit differences from Lainey.

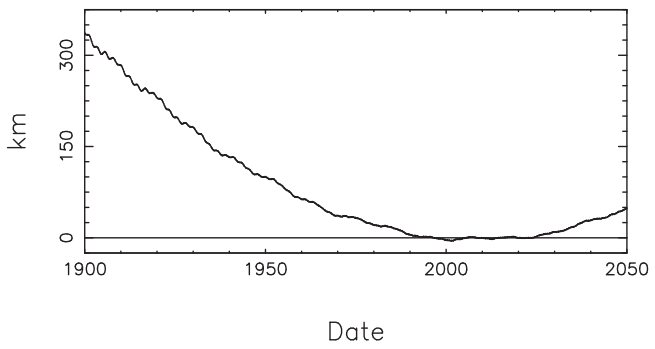

Figure 10. Enceladus in-orbit differences from Lainey.

uncertainty exceeds it value. Clearly, the tracking data are important, but extremely so for Titan.

Lainey et al. (2020) performed an analysis analogous to ours. They employed two independent methods: (1) a fit of all of the satellite orbits to Earth-based astrometry and Cassini imaging, and (2) a fit of only the Titan orbit to the Cassini tracking data during the 10 Titan gravity science flybys. Their first method yielded results similar to ours in Table 11. The second method found a larger Q_{Si} associated with Titan, but its value, 124, was nearly an order of magnitude smaller than ours from Table 10.

We have some concern about their second method in which they estimated Titan's state, Titan's gravity field, Saturn's gravity field, Love number, and Q. Whereas the flyby tracking data are crucial in the determination of Titan's orbit and

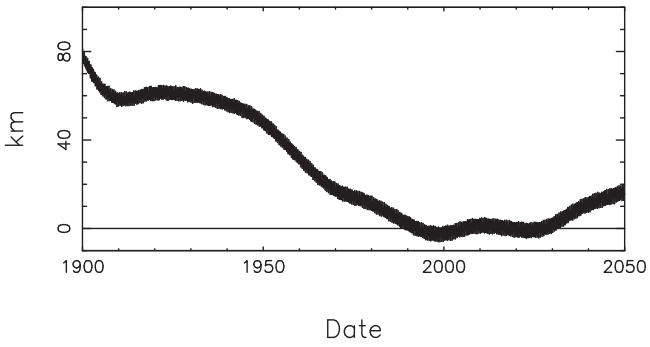

Figure 11. Tethys in-orbit differences from Lainey.

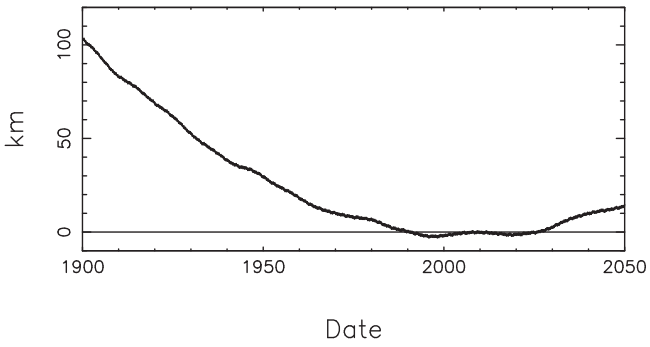

Figure 12. Dione in-orbit differences from Lainey.

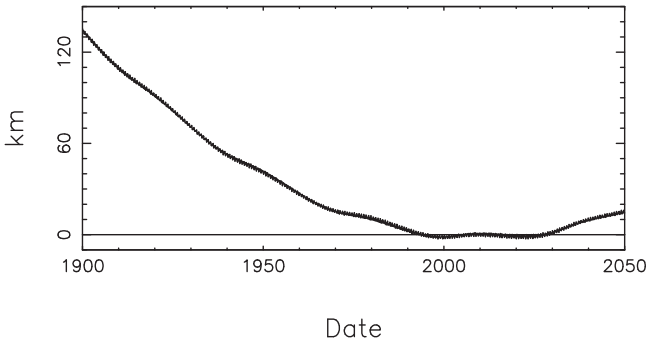

Figure 13. Rhea in-orbit differences from Lainey.

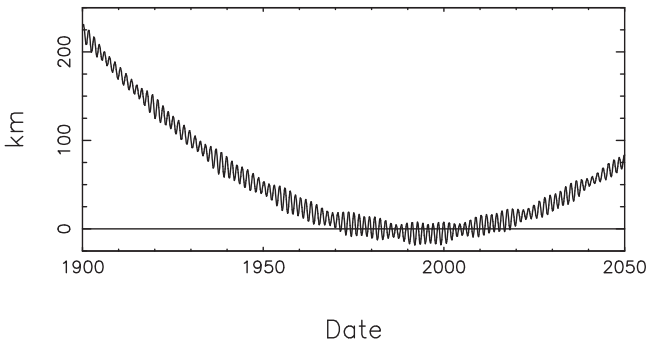

Figure 14. Titan in-orbit differences from Lainey.

gravity, they do not provide a good estimate of Saturn's gravity field or Love number. Moreover, we believe that the time span of the data may be too short to separate any tidal acceleration from long-term periodic gravitational perturbations. We were unable to replicate the result from the fit to the Titan flyby data as outlined by Lainey et al. (2020). However, when we estimated only Titan's state and gravity field, Saturn's *GM*, and

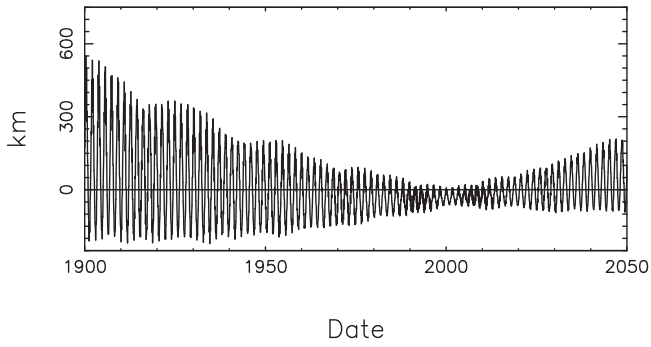

Figure 15. Hyperion in-orbit differences from Lainey.

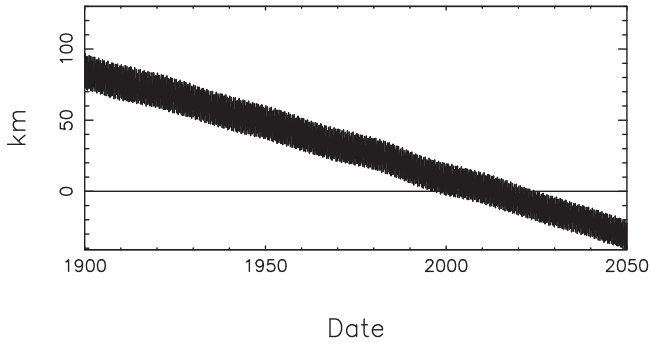

Figure 16. Iapetus in-orbit differences from Lainey.

Titan lag time (taking Saturn's gravity field and Love number as known) from the flyby data, we obtained the indeterminate nonphysical $\Delta t = -0.276 \pm 0.968$ s. Combining the flyby data with the Earth-based astrometry and imaging yielded little change, but adding the Voyager 1 flyby data produced $\Delta t = 1.613 \pm 0.410$ s. We conclude that the Titan tidal acceleration is quite small such that the constraint placed on the Titan orbit by the Voyager 1 flyby and all 127 Cassini flybys is necessary to detect it.

4.7. Descriptive Elements

The orbit geometries (general size, shape, orientation) can be roughly represented by the average values of the planetocentric osculating elements derived from the integrated orbits (for Phoebe a better representation is barycentric). We refer the elements to the satellites' Laplace planes. These are planes lying between the Saturn equator and Saturn orbit; on average, the satellite orbits maintain constant inclinations to the Laplace planes. For orbits interior to Titan, the Laplace planes are effectively identical to the Saturn equator. The elements of the current orbits appear in Table 12; they are as follows: a—semimajor axis, e—eccentricity, i—inclination to the Laplace plane. The precession periods of the periapsis and node are P_ω and P_Ω. The inclination of the Laplace plane to the Saturn equator is ϵ.

4.8. Orbit Accuracy

Table 13 gives our assessment of the 1σ orbital uncertainties at the time of the end of the Cassini mission and at about the time of the proposed Dragonfly mission (Lorenz et al. 2018) in the direction along the radius from Saturn, the direction along the orbital track, and the direction normal to the orbital plane. For all of the satellites the normal uncertainties are fairly

Table 14
Visual Micrometer Observation Residuals

Type	No.	rms	Type	No.	Rms	Dates	Source
ρ	75	1.″047	θ	116	1.″096	1875	AstronomerRoyal (1876)
ρ	644	0.″524	θ	603	0.″524	1874–1883	USNO (1877–87)
$\Delta\alpha\cos\delta$	3	1.″165	$\Delta\delta$	2	0.″517	1878	USNO (1877–87)
$\Delta\alpha$	169	0.″635	$\Delta\delta$	190	0.″333	1875–1877	USNO (1877–87)
ρ	14	1.″831	θ	10	1.″444	1879	Common (1879)
ρ	337	0.″690	θ	322	0.″654	1883–1889	USNO (1887,1889-93)
$\Delta\alpha$	28	0.″436	$\Delta\delta$	30	0.″245	1889	USNO (1887,1889-93)
$\Delta\alpha$	26	0.″984	$\Delta\delta$	30	0.″656	1887	von Engelhardt (1887)
$\Delta\alpha$	1	0.″324	$\Delta\delta$	3	0.″283	1888	von Engelhardt (1888)
ρ	12	0.″238	θ	12	0.″371	1888	von Engelhardt (1888)
ρ	21	0.″257	θ	21	0.″315	1890	von Engelhardt (1890)
$\Delta\alpha$	2	0.″253	$\Delta\delta$	6	0.″824	1890	von Engelhardt (1890)
$\Delta\alpha\cos\delta$	101	0.″129	$\Delta\delta$	96	0.″122	1886–1892	Struve (1898)
ρ	1015	0.″249	θ	1000	0.″182	1886–1892	Struve (1898)
ρ	415	0.″347	θ	402	0.″323	1896–1901	Hussey (1902)
ρ	388	0.″378	θ	397	0.″295	1902	Hussey (1903)
ρ	219	0.″266	θ	216	0.″240	1904	Hussey (1905)
ρ	38	0.″200	θ	40	0.″164	1905	Aitken (1906)
ρ	23	0.″128	θ	21	0.″205	1907	Aitken (1909)
ρ	27	0.″168	θ	49	0.″176	1906–1908	Barnard (1910)
ρ	1850	0.″260	θ	1854	0.″269	1894–1907	USNO (1911)
$\Delta\alpha$	161	0.″479	$\Delta\delta$	157	0.″322	1894–1907	USNO (1911)
ρ	145	0.″268	θ	291	0.″250	1910–1912	Barnard (1912)
ρ	122	0.″306	θ	120	0.″233	1912–1913	Barnard (1913a)
ρ	81	0.″272	θ	78	0.″221	1913–1914	Barnard (1915)
ρ	108	0.″230	θ	109	0.″200	1915–1916	Barnard (1916)
ρ	113	0.″265	θ	112	0.″198	1916–1917	Barnard (1918)
ρ	30	0.″223	θ	31	0.″278	1919	Godard (1919)
ρ	343	0.″238	θ	338	0.″209	1917–1922	Barnard (1927)
ρ	1243	0.″181	θ	1232	0.″185	1908–1926	USNO (1929)
$\Delta\alpha$	43	0.″437	$\Delta\delta$	46	0.″285	1908–1915	USNO (1929)
ρ	2046	0.″196	θ	2037	0.″178	1916–1928	Struve (1933)
$\Delta\alpha$	0		$\Delta\delta$	2	0.″294	1918	Struve (1933)
ρ	1216	0.″207	θ	1227	0.″225	1927–1947	Hall et al. (1954)
$\Delta\alpha\cos\delta$	32	0.″311	$\Delta\delta$	32	0.″179	1930	Hall et al. (1954)

constant, and for all but Mimas, Hyperion, and Phoebe the radial uncertainties have little or no variation. The increasing uncertainties in the downtrack direction are a consequence of error in the satellites' mean motion.

4.9. Orbit Comparisons

The satellite ephemerides used to support the Cassini tour and its reconstruction did not account for the quadrupole fields of the satellites, the tidal dissipation in Saturn or Enceladus, or the Lense–Thirring relativistic effect. Figures 1–8 show the in-orbit differences between the final reconstruction ephemeris, SAT427, and the current ephemerides for the time frame of the tour. The differences are small for those satellites that had Cassini flybys, namely, Enceladus, Dione, Rhea, and Titan. The effect of the tidal dissipation is evident by the "parabolic" nature of the differences for Tethys, Dione, Rhea, and Titan. The lack of a significant Enceladus tidal signature suggests a balance between the dissipation in Saturn and that in Enceladus. The strong mean motion resonance between Mimas and Tethys has probably limited the direct effect of the tide on the Mimas orbit. The periodic signature in the Hyperion orbit is a consequence of the difference in the 21-month mean motion resonance with Titan. The two Iapetus orbits have slightly different mean motions.

Figures 9–16 display the differences in in-orbit positions between our ephemeris and that of Lainey et al. (2020; NOE-6-2018-MAIN-v2). The latter is available from Institut de Mécanique Céleste et de Calcul des Ephémérides as an alternate Saturnian satellite ephemeris. Both are in fair agreement during the time frame of the Cassini tour (2004–2017); however, the differences clearly show the effects of differing tide models. Hyperion and Iapetus are not tidally accelerated in either ephemeris. The former is strongly perturbed by Titan, and presumably the differences in the Titan orbits account for the periodic differences in its orbit. The Iapetus difference simply reflects slight differences between the mean motions in the two ephemerides.

5. Observation Residuals

The rms of the residuals for the main satellite Earth-based observations are listed for each data set in Tables 14–17. The tables include the type, number, and time span of the set. The types are as follows:

α, δ: R.A. and decl. of the satellite;
$\Delta\alpha$, $\Delta\delta$: differential R.A. and decl. of the satellite relative to a reference body;
$\Delta\alpha\cos\delta$: differential R.A. scaled by the cosine of the decl. of the reference body;

Table 15
Photographic and CCD Astrometric Observation Residuals

Type	No.	rms	Type	No.	Rms	Dates	Source
$\Delta\alpha \cos\delta$	294	0.″117	$\Delta\delta$	289	0.″103	1926	Alden & O'Connell (1928)
$\Delta\alpha \cos\delta$	176	0.″092	$\Delta\delta$	178	0.″104	1927	Alden (1929)
$\Delta\alpha$	38	0.″249	$\Delta\delta$	38	0.″183	1967	Soulie (1968)
$\Delta\alpha$	130	0.″335	$\Delta\delta$	130	0.″270	1968–1969	Soulie (1972)
$\Delta\alpha$	6	0.″267	$\Delta\delta$	6	0.″318	1971	Peters (1973)
$\Delta\alpha$	144	0.″185	$\Delta\delta$	144	0.″131	1972–1973	Sinclair (1974)
ρ	18	0.″985	θ	34	0.″642	1970–1971	Soulie (1975)
$\Delta\alpha$	76	0.″395	$\Delta\delta$	77	0.″274	1970–1971	Soulie (1975)
$\Delta\alpha$	59	0.″117	$\Delta\delta$	59	0.″099	1972	Abbot et al. (1975)
$\Delta\alpha$	47	0.″287	$\Delta\delta$	47	0.″249	1972	Kisseleva et al. (1975)
$\Delta\alpha$	79	0.″156	$\Delta\delta$	79	0.″288	1973	Mulholland et al. (1976)
$\Delta\alpha$	223	0.″151	$\Delta\delta$	223	0.″146	1972–1974	Kisseleva et al. (1977)
$\Delta\alpha$	132	0.″115	$\Delta\delta$	132	0.″111	1972–1976	Sinclair (1977)
$\Delta\alpha$	66	0.″380	$\Delta\delta$	66	0.″276	1972–1974	Soulie (1978)
ρ	25	0.″431	θ	24	0.″475	1972–1974	Soulie (1978)
$\Delta\alpha$	1	0.″145	$\Delta\delta$	1	0.″576	1977	Walker et al. (1978)
$\Delta\alpha$	14	0.″488	$\Delta\delta$	14	0.″348	1977	Debehogne (1979)
$\Delta\alpha$	30	0.″244	$\Delta\delta$	30	0.″231	1975	Levitskaya (1979)
$\Delta\alpha \cos\delta$	105	0.″152	$\Delta\delta$	105	0.″298	1978	Seitzer et al. (1979)
$\Delta\alpha$	60	0.″109	$\Delta\delta$	60	0.″087	1978	Seitzer et al. (1979)
$\Delta\alpha$	122	0.″162	$\Delta\delta$	122	0.″143	1975–1976	Mulholland & Shelus (1980)
$\Delta\alpha$	12	0.″298	$\Delta\delta$	12	0.″501	1978	Chugunov & Nefedev (1980)
$\Delta\alpha$	44	0.″388	$\Delta\delta$	44	0.″385	1980	Kitkin & Chugunov (1980)
$\Delta\alpha \cos\delta$	28	0.″123	$\Delta\delta$	28	0.″395	1977	Seitzer & Ianna (1980)
$\Delta\alpha$	49	0.″184	$\Delta\delta$	49	0.″142	1977	Seitzer & Ianna (1980)
$\Delta\alpha$	52	0.″434	$\Delta\delta$	52	0.″486	1977–1978	Chugunov (1981)
$\Delta\alpha$	62	0.″444	$\Delta\delta$	62	0.″297	1975–1976	Soulie et al. (1981)
$\Delta\alpha$	9	0.″421	$\Delta\delta$	9	0.″285	1981	Debehogne (1981, 1982)
$\Delta\alpha \cos\delta$	1142	0.″095	$\Delta\delta$	1142	0.″096	1974–1980	Pascu (1982)
$\Delta\alpha$	63	0.″332	$\Delta\delta$	63	0.″335	1981	Kitkin & Chugunov (1982)
$\Delta\alpha \cos\delta$	357	0.″306	$\Delta\delta$	357	0.″311	1979–1981	Rohde et al. (1982)
$\Delta\alpha$	307	0.″216	$\Delta\delta$	307	0.″124	1979–1981	Rohde et al. (1982)
$\Delta\alpha$	65	0.″269	$\Delta\delta$	65	0.″307	1982	Debehogne (1984)
$\Delta\alpha$	183	0.″172	$\Delta\delta$	183	0.″170	1977–1983	Taylor & Sinclair (1985)
$\Delta\alpha$	350	0.″234	$\Delta\delta$	350	0.″244	1981	Dourneau et al. (1985)
$\Delta\alpha$	69	0.″414	$\Delta\delta$	69	0.″427	1982–1984	Kitkin (1985)
$\Delta\alpha$	399	0.″114	$\Delta\delta$	399	0.″081	1981	Dourneau et al. (1986)
$\Delta\alpha \cos\delta$	40	0.″251	$\Delta\delta$	40	0.″213	1982–1984	Kisseleva et al. (1987)
$\Delta\alpha$	17	0.″107	$\Delta\delta$	17	0.″164	1982–1984	Kisseleva et al. (1987)
$\Delta\alpha$	7	0.″312	$\Delta\delta$	7	0.″422	1981–1982	Bowell (1988)
$\Delta\alpha$	55	0.″191	$\Delta\delta$	55	0.″172	1987–1988	Shen (1988)
$\Delta\alpha \cos\delta$	472	0.″303	$\Delta\delta$	472	0.″233	1984	Dourneau et al. (1989)
$\Delta\alpha \cos\delta$	534	0.″094	$\Delta\delta$	533	0.″165	1975–1982	Tolbin (1991a)
$\Delta\alpha$	369	0.″088	$\Delta\delta$	369	0.″116	1975–1982	Tolbin (1991a)
$\Delta\alpha$	550	0.″231	$\Delta\delta$	550	0.″222	1973–1984	Tolbin (1991b)
$\Delta\alpha$	229	0.″230	$\Delta\delta$	229	0.″198	1980	Izhakevich (1991)
$\Delta\alpha \cos\delta$	1159	0.″142	$\Delta\delta$	1159	0.″105	1980–1985	Veillet & Dourneau (1992)
$\Delta\alpha$	149	0.″215	$\Delta\delta$	149	0.″232	1992–1994	Whipple (1992, 1993, 1995)
$\Delta\alpha \cos\delta$	14	0.″097	$\Delta\delta$	14	0.″109	1992	Rohde & Pascu (1993)
$\Delta\alpha \cos\delta$	14	0.″076	$\Delta\delta$	14	0.″111	1990–1993	Nicholson (1994)
$\Delta\alpha \cos\delta$	764	0.″219	$\Delta\delta$	764	0.″222	1970–1972	Hatanaka (1995)
$\Delta\alpha$	494	0.″154	$\Delta\delta$	494	0.″139	1973–1985	Standish (1996)
$\Delta\alpha \cos\delta$	143	0.″104	$\Delta\delta$	143	0.″282	1994–1995	Kisseleva et al. (1996)
x	1238	0.″296	y	1238	0.″276	1990–1994	Harper et al. (1997)
$\Delta\alpha \cos\delta$	2497	0.″169	$\Delta\delta$	2495	0.″161	1995	Vass (1997)
$\Delta\alpha \cos\delta$	35	0.″113	$\Delta\delta$	35	0.″404	1996	Kisseleva & Kalinitchenko (1998)
$\Delta\alpha$	773	0.″266	$\Delta\delta$	773	0.″218	1982–1988	Veiga & Vieira Martins (1999)
x	610	0.″163	y	610	0.″204	1994–1999	Qiao et al. (1999)
x	1454	0.″139	y	1454	0.″161	1995–1997	Harper et al. (1999)
α	626	0.″211	δ	626	0.″159	1973–1997	Krasinsky (2000)
$\Delta\alpha \cos\delta$	57	0.″225	$\Delta\delta$	57	0.″236	1995–2000	Kisseleva & Izmailov (2000)
$\Delta\alpha \cos\delta$	92	0.″103	$\Delta\delta$	92	0.″141	1997–1999	Kisseleva & Kalinitchenko (2000)
α	411	0.″166	δ	411	0.″202	1998–1999	Stone & Harris (2000)
α	420	0.″179	δ	420	0.″192	1999–2000	Stone (2000)

Table 15
(Continued)

Type	No.	rms	Type	No.	Rms	Dates	Source
$\Delta\alpha$	9	0.″703	$\Delta\delta$	9	0.″429	1978–1984	Izhakevich (2001)
$\Delta\alpha$	382	0.″309	$\Delta\delta$	382	0.″264	1961–1984	Filippov (2001)
$\Delta\alpha\cos\delta$	6000	0.″081	$\Delta\delta$	6000	0.″069	1995	Vienne et al. (2001)
$\Delta\alpha\cos\delta$	202	0.″029	$\Delta\delta$	202	0.″024	1995	McGhee et al. (2001)
α	362	0.″135	δ	362	0.″124	2000–2001	Stone (2001)
$\Delta\alpha\cos\delta$	115	0.″124	$\Delta\delta$	115	0.″170	1999–2001	Kisseleva & Kalinitchenko (2002)
$\Delta\alpha\cos\delta$	913	0.″052	$\Delta\delta$	913	0.″048	1996–2000	Peng et al. (2002)
$\Delta\alpha\cos\delta$	25	0.″034	$\Delta\delta$	25	0.″018	1995	French et al. (2003)
$\Delta\alpha\cos\delta$	2010	0.″116	$\Delta\delta$	2010	0.″096	1995–1999	Veiga et al. (2003)
x	1166	0.″428	y	1166	0.″358	1997–2000	Qiao et al. (2004)
$x_{\rm pc}$	275	0.″017	$y_{\rm pc}$	275	0.″011	1996–2005	French et al. (2006)
$x_{\rm wf}$	821	0.″024	$y_{\rm wf}$	821	0.″026	1996–2005	French et al. (2006)
α	1211	0.″111	δ	1211	0.″114	2001–2005	Stone (2001–2005)
$\Delta\alpha\cos\delta$	1792	0.″048	$\Delta\delta$	1792	0.″053	2002–2006	Peng et al. (2008)
α	463	0.″114	δ	463	0.″137	2005–2007	Monet (2005–2007)
$\Delta\alpha\cos\delta$	434	0.″109	$\Delta\delta$	434	0.″127	2002–2008	Kisseleva (2009), Khrutskaya et al. (2009)
$\Delta\alpha\cos\delta$	75	0.″120	$\Delta\delta$	75	0.″093	2008–2009	Grosheva et al. (2011)
α	1395	0.″150	δ	1395	0.″151	2007–2016	Harris (2007–2016)
α	840	0.″116	δ	840	0.″077	2002–2017	Owen (2018)

Table 16
Mutual Event Residuals

Type	No.	rms	Type	No.	Rms	Dates	Source
$\Delta\alpha\cos\delta$	11	0.″010	$\Delta\delta$	11	0.″019	1979–1980	Aksnes et al. (1984)
$\Delta\alpha\cos\delta$	51	0.″037	$\Delta\delta$	51	0.″045	1980–1996	Noyelles et al. (2003)
$\Delta\alpha\cos\delta$	26	0.″082	$\Delta\delta$	26	0.″022	2008–2009	Arlot et al. (2012)

Table 17
Transit and Occultation Residuals

Type	No.	rms	Type	No.	Rms	Dates	Source
α	80	0.″172	δ	80	0.″317	1985–1992	Rapaport (1989, 1992)
α	710	0.″223	δ	710	0.″193	1987–1997	Carlsberg Meridian Cat (1999)
α	130	0.″131	δ	130	0.″187	1997–2000	Rapaport et al. (2002)
α	171	0.″088	δ	171	0.″109	2001–2007	Arlot et al. (2008)
α	3	0.″018	δ	3	0.″001	1974–2014	Herald et al. (2020)

Table 18
Lagrangian Satellite Astrometric Observation Residuals

Type	No.	rms	Type	No.	Rms	Dates	Source
			θ	1	0.″133	1980	Leliévre (1980)
			θ	4	0.″546	1980	Laques et al. (1980)
ρ_r	5	0.″584	z_r	5	0.″336	1980	Lamy & Mauron (1980)
			θ	1	0.″157	1980	Retisema et al. (1980)
			θ	1	0.″481	1980	Veillet (1980)
ρ_r	14	0.″408				1980	Seidelmann et al. (1981)
ρ_r	57	0.″421				1980–1981	Reitsema (1981)
$\Delta\alpha$	2	0.″305	$\Delta\delta$	2	0.″048	1981	Pascu & Seidelmann (1981)
$\Delta\alpha$	1	0.″004	$\Delta\delta$	1	0.″446	1981	Larson & Fountain (1981)
$\Delta\alpha\cos\delta$	271	0.″335	$\Delta\delta$	271	0.″275	1981–1985	Oberti et al. (1989)
$\Delta\alpha\cos\delta$	104	0.″288	$\Delta\delta$	104	0.″182	1992	Rohde & Pascu (1993)
$\Delta\alpha\cos\delta$	69	0.″291	$\Delta\delta$	69	0.″287	1992–1994	Martinka & Pascu (1998)
$\Delta\alpha\cos\delta$	79	0.″122	$\Delta\delta$	79	0.″134	1993	Rohde & Pascu (1994)
$\Delta\alpha\cos\delta$	21	0.″437	$\Delta\delta$	21	0.″239	1985–1987	Veiga & Vieira Martins (2000)
$\Delta\alpha\cos\delta$	51	0.″087	$\Delta\delta$	51	0.″053	1995	McGhee et al. (2001)
$\Delta\alpha\cos\delta$	4	0.″053	$\Delta\delta$	4	0.″082	1995	French et al. (2003)
$\Delta\alpha\cos\delta$	74	0.″633	$\Delta\delta$	74	0.″867	1995–1996	Veiga et al. (2003)
$x_{\rm wf}$	366	0.″026	$y_{\rm wf}$	366	0.″032	1996–2005	French et al. (2006)
$x_{\rm pc}$	28	0.″023	$y_{\rm pc}$	28	0.″020	1997–2001	French et al. (2006)

Table 19
Phoebe Astrometric Observation Residuals

Type	No.	rms	Type	No.	Rms	Dates	Source
α	29	7.″757	δ	29	5.″049	1898–1902	Pickering (1908)
α	5	0.″935	δ	5	0.″523	1904	Perrine (1904)
ρ	26	4.″505	$\Delta\delta$	26	7.″279	1904	Pickering (1905a, 1905b)
ρ	11	11.″497	$\Delta\delta$	11	13.″630	1905	Pickering (1906a)
α	11	0.″889	δ	11	1.″646	1905	Albrecht & Smith (1909)
α	11	3.″952	δ	12	1.″471	1906	Barnard (1908a)
ρ	6	3.″399	$\Delta\delta$	6	9.″139	1906	Pickering (1906b)
ρ	9	7.″605	$\Delta\delta$	9	5.″413	1906	Pickering (1906c)
α	10	0.″543	δ	10	0.″484	1906–1908	Perrine (1909)
α	19	0.″692	δ	19	1.″163	1907	Christie (1909)
α	27	0.″854	δ	27	0.″920	1908	Christie (1910)
α	14	1.″072	δ	14	0.″929	1909–1910	Christie (1911)
α	8	1.″343	δ	8	0.″680	1910	Christie (1912)
α	12	1.″199	δ	7	1.″141	1912–1913	Barnard (1913b)
α	5	0.″639	δ	3	0.″389	1913	Barnard (1914)
α	4	1.″001	δ	4	1.″209	1922	van Biesbroeck (1922)
α	1	0.″287	δ	1	0.″009	1940	Richmond & Nicholson (1943)
α	7	0.″618	δ	7	0.″242	1942	van Biesbroeck (1944)
α	7	0.″939	δ	7	0.″307	1952	Bobone (1953)
α	11	0.″860	δ	11	0.″566	1955	van Biesbroeck (1956)
α	8	0.″681	δ	8	0.″693	1957	van Biesbroeck (1958)
α	2	0.″310	δ	2	0.″124	1960	Roemer & Lloyd (1966)
α	2	1.″383	δ	2	0.″594	1968	Chernykh & Chernykh (1971)
α	2	0.″983	δ	2	0.″289	1969	van Biesbroeck et al. (1976)
$\Delta\alpha$	9	0.″344	$\Delta\delta$	9	0.″168	1976	Mulholland & Shelus (1980)
$\Delta\alpha$	21	0.″539	$\Delta\delta$	21	0.″546	1981	Debehogne (1981, 1982)
$\Delta\alpha$	11	1.″032	$\Delta\delta$	11	1.″023	1981	Bowell (1988)
$\Delta\alpha$	18	0.″534	$\Delta\delta$	18	0.″590	1982	Debehogne (1984)
α	5	0.″150	δ	5	0.″220	1989	Dourneau et al. (1991)
α	31	0.″350	δ	31	0.″201	1992–1993	Rohde (1994)
α	49	0.″574	δ	49	0.″335	1992–1996	Whipple (1992, 1993, 1995, 1996)
α	3	0.″598	δ	3	0.″454	1994	Nicholson (2000)
α	7	0.″089	δ	7	0.″157	1995–1997	Jones (1999)
α	60	0.″178	δ	60	0.″404	1995–1997	Veiga et al. (2000)
α	1082	0.″485	δ	1082	0.″536	1995–2019	MPC (2000–2019)
α	1683	0.″053	δ	1683	0.″055	1996–2014	Gomes-Júnior et al. (2015)
α	29	0.″654	δ	29	0.″440	1997–1998	Shelus (1998)
α	9	0.″074	δ	9	0.″090	1998	Ledovskaya et al. (1999)
α	38	0.″222	δ	38	0.″348	1998–1999	Stone & Harris (2000)
α	162	0.″153	δ	162	0.″187	1998–1999	Fienga et al. (2002)
α	24	0.″266	δ	24	0.″212	1999–2000	Stone (2000)
$\Delta\alpha$	3	0.″161	$\Delta\delta$	3	0.″196	2000	Gladman et al. (2000)
α	22	0.″179	δ	22	0.″259	2000–2001	Stone (2001)
α	3	0.″507	δ	3	0.″424	2001	Kowalski (2001)
α	100	0.″291	δ	100	0.″292	2001–2005	Stone (2001–2005)
α	147	0.″092	δ	147	0.″112	2001–2016	Owen (2018)
α	115	0.″116	δ	115	0.″151	2003–2004	Qiao et al. (2006)
α	210	0.″054	δ	210	0.″050	2003–2005	Peng & Zhang (2006)
α	27	0.″412	δ	27	0.″273	2005–2006	Monet (2005–2007)
α	1173	0.″110	δ	1173	0.″102	2005–2008	Qiao et al. (2011)
α	95	0.″283	δ	95	0.″417	2008–2015	Harris (2007–2016)
α	346	0.″038	δ	346	0.″034	2011–2014	Peng et al. (2015)

ρ, θ: planet relative separation and position angle (position angle residuals are scaled by the associated separation);
x, y: CCD sample and line locations;
x_{pc}, y_{pc}: HST x, y measures, PC chip;
x_{wf}, y_{wf}: HST x, y measures, WF chip.

Table 18 provides the analogous information for the Lagrangian satellite Earth-based astrometric observations; the additional data type (ρ_r, z_r) is planet-relative separation measured in the ring plane and the distance normal to the ring plane. The Phoebe residual statistics appear in Table 19, and the statistics for the Voyager and Cassini imaging data grouped by satellite are contained in Table 20.

Figure 17 shows the residuals for the ring occultation data as a function of time. The overall rms is 382 m and is compatible with that obtained by French et al. (2017). Figure 18 displays the residuals for the ring position angles. The observer noted that most of the observations in 1906–1908 were made under poor to fair seeing conditions; seeing was better in 1891–1892.

Table 20
Imaging Residuals (pixels)

Satellite	Voyager 1			Voyager 2			Cassini		
	No.	Sample	Line	No.	Sample	Line	No.	Sample	Line
Mimas	42	0.198	0.249	47	0.229	0.306	538	0.443	0.397
Enceladus	33	0.264	0.211	57	0.288	0.236	736	0.411	0.371
Tethys	42	0.173	0.376	64	0.205	0.373	521	0.371	0.434
Dione	42	0.281	0.275	55	0.249	0.293	525	0.388	0.404
Rhea	49	0.275	0.242	35	0.234	0.348	600	0.321	0.404
Titan	57	0.394	0.419	29	0.254	0.248			
Hyperion	9	0.320	0.361	9	0.173	0.224	246	1.227	0.943
Iapetus				5	0.198	0.193	309	0.432	0.480
Phoebe				9	0.248	0.489	156	0.145	0.200
Helene	4	0.143	0.594	13	0.420	0.576	633	0.221	0.250
Telesto				11	0.188	0.458	581	0.191	0.191
Calypso				12	0.345	0.645	505	0.196	0.219
Polydeuces							335	0.228	0.249
Methone							389	0.922	0.940

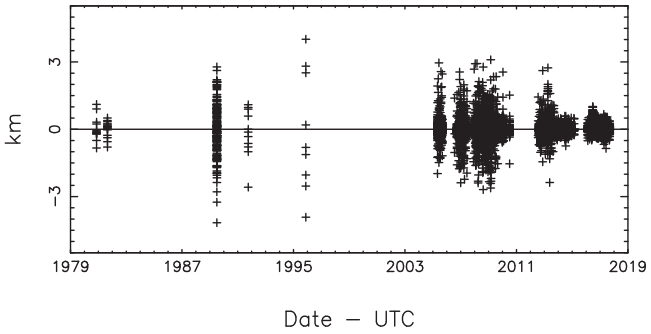

Figure 17. Ring radius residuals.

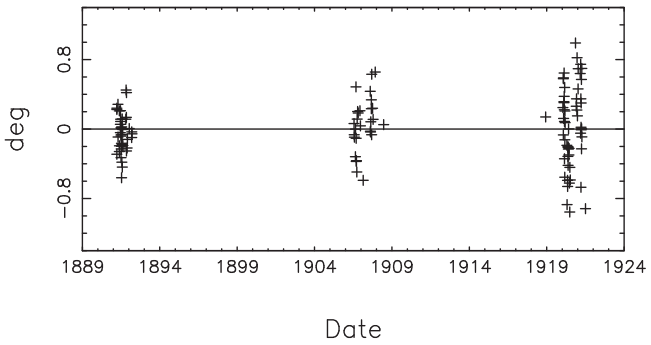

Figure 18. Ring position angle residuals.

No notes are available concerning the seeing in 1920–1921. Although the position angle measures are not highly accurate, the 1891 data confirm that our pole precession cannot be too far off.

The observed ring plane crossing times and their residuals for our pole orientation appear in Table 21, along with the residuals for the pole model of French et al. (2017). The 1907–1908 crossing times were inferred from visually observed disappearance and reappearance times, and we arbitrarily assigned their accuracies. The 1966 crossing was observed photographically, and the accuracies were provided by the observers. The 1995 crossing was observed with HST. The disparity between the quoted accuracy and the residuals is almost exactly 3σ for the May observation and a bit more than 1σ for the August observation. Overall the fit to the crossing times is not too bad considering the difficulty in determining a single time at which the observer passed through the ring plane. Moreover, we are using a simple model for our calculation of the crossing time, i.e., the time at which the geometric direction from the observer to Saturn is normal to the pole vector.

Table 21
Ring Plane Crossing Times

Observed Time	Resid	
	French et al.	Current
1907 Oct 3 10:30:00 ± 1:00:00 GMT	−1:25:53	−1:24:39
1908 Jan 7 08:15:00 ± 2:00:00 GMT	1:04:05	1:02:08
1966 Dec 18 05:18:00 ± 3:18:00 UTC	−3:47:18	−3:53:52
1966 Dec 18 07:00:00 ± 1:55:00 UTC	−2:05:07	−2:11:40
1995 May 22 05:34:00 ± 0:02:20 UTC	0:09:42	0:06:59
1995 Aug 10 21:00:00 ± 0:20:00 UTC	0:21:32	0:24:31

Figure 19 displays the Cassini range residuals. The range measures distance along the Earth–spacecraft direction. It is sensitive to the Saturn position relative to Earth, the spacecraft position relative to Saturn, and spacecraft position relative to the satellites during close flybys. The Cassini tour contained 291 orbits of Saturn, 127 flybys of Titan, 23 of Enceladus, 6 of Rhea, 5 of Dione, and 1 each of Tethys, Hyperion, and Phoebe. The range residuals add confirmation that the Saturn orbit (from DE440), the satellite orbits, and the Cassini spacecraft trajectory are well determined.

6. Concluding Remarks

In this article we have reported on an extensive post-Cassini data analysis leading to revised orbits for the major Saturnian satellites. As a requisite part of the work we determined the Saturnian system gravity field, i.e., the *GM*s of the planet and satellites, as well as the gravitational harmonics of the planet, Enceladus, Dione, Rhea, and Titan. We also obtained estimates for Saturn's tidal Love number, its tidal dissipation at the orbital frequencies of its six largest satellites, its pole orientation, and its axial moment of inertia.

The ephemerides for the satellites based on this analysis are available electronically from the On-Line Solar System Data Service at the Jet Propulsion Laboratory (Giorgini et al. 1996)

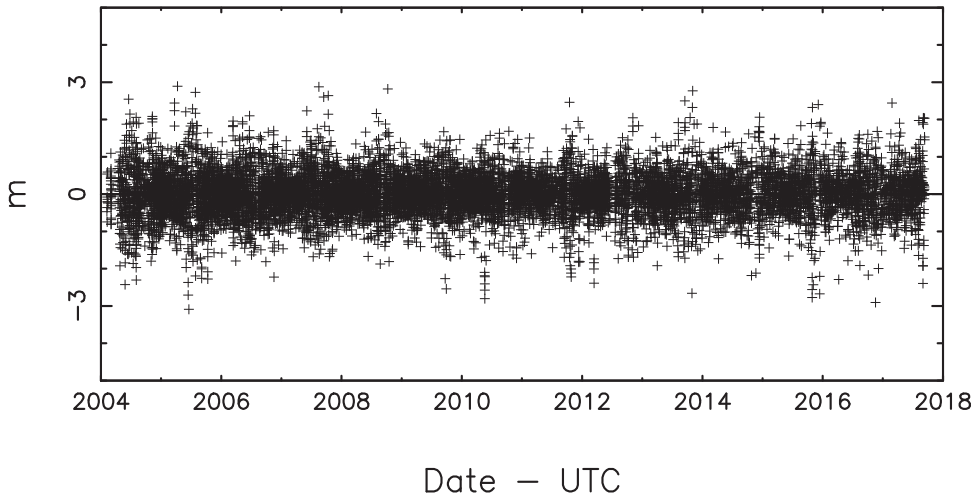

Figure 19. Cassini range residuals.

and NASA's Navigation and Ancillary Information Facility (NAIF; Acton 1996); their designation is SAT441. The trajectories for the spacecraft that accompany the ephemerides may also be obtained from NAIF.

I would like to thank B. Folkner and B. Owen for their assistance with this work. I am indebted to D. Roth, J. Bellerose, Cassini Navigation Team, the Cassini Imaging Science Team, and the Cassini Radio Science Team for help with the Cassini data processing. R. French provided invaluable ring occultation measurements and assistance in their analysis. P. Nicholson assisted me with the ring plane crossing timings. The research described here was carried out at the Jet Propulsion Laboratory, California Institute of Technology, under contract with the National Aeronautics and Space Administration (80NM0018D0004).

Appendix

The model for the motion of the pole of Saturn is based on the rotational equations of motion for a rigid body. The equations assume that the planet is axially symmetric and that the torques applied are derived from the Sun and q satellites acting on the planet's figure as represented by its zonal gravitational harmonics. The equations are

$$\frac{d\hat{\boldsymbol{k}}}{dt} = \frac{1}{\gamma s R^3}\sum_{n=2}^{\infty} J_n \left[\mu_\odot \left(\frac{R}{r_\odot}\right)^{n+1} P_n'(\hat{\boldsymbol{r}}_\odot \cdot \hat{\boldsymbol{k}})(\hat{\boldsymbol{r}}_\odot \times \hat{\boldsymbol{k}}) + \sum_{j=1}^{q} \mu_j \left(\frac{R}{r_j}\right)^{n+1} P_n'(\hat{\boldsymbol{r}}_j \cdot \hat{\boldsymbol{k}})(\hat{\boldsymbol{r}}_j \times \hat{\boldsymbol{k}}) \right],$$

where $\hat{\boldsymbol{k}}$ = Saturn's pole vector, γ = Saturn's normalized axial moment of inertia, R = Saturn's equatorial radius, s = Saturn's rotation rate, J_n = Saturn's nth zonal gravity harmonic, $P_n'(x)$ = the derivative of the Legendre polynomial of degree n with argument x, $\mu_\odot = GM$ of the Sun, $\mu_j = GM$ of satellite j, $\boldsymbol{r}_\odot$ = the Saturn-centered position of the Sun, $\boldsymbol{r}_j$ = the Saturn-centered position of satellite j, and r_j and $\hat{\boldsymbol{r}}_j$ are the magnitude and direction of $\boldsymbol{r}_j$.

References

Abbot, R. I., Mulholland, J. D., & Shelus, P. J. 1975, AJ, 80, 723
Acton, C. H., Jr. 1996, P&SS, 44, 65
Aitken, R. G. 1906, LicOB, 94, 31
Aitken, R. G. 1909, LicOB, 172, 169
Aksnes, K., Franklin, F., Millis, R., et al. 1984, AJ, 89, 280
Albrecht, S., & Smith, E. 1909, LicOB, 156, 109
Alden, H. L. 1929, AJ, 40, 88
Alden, H. L., & O'Connell, W. C. 1928, AJ, 38, 53
Anderson, J. D., & Schubert, G. 2007, AGUFM, 2007, P54A–05
Antreasian, P., Ardalan, S., Bordi, J., et al. 2008, Cassini Orbit Determination Results January 2006–End of Prime Mission, AIAA Paper 2008-6747, AIAA/AAS Astrodynamics Specialist Conference and Exhibit (San Diego, CA: AIAA)
Archinal, B. A., Acton, C. H., A'Hearn, M. F., et al. 2018, CeMec, 130, 22
Arlot, J. E., Dourneau, G., & Le Campion, J. F. 2008, A&A, 484, 869
Arlot, J.-E., & Emelyanov, N. V. 2009, A&A, 503, 631
Arlot, J.-E., Emelyanov, N. V., Lainey, V., et al. 2012, A&A, 544, A29
AstronomerRoyal 1876, MNRAS, 36, 266
Bar-Sever, Y., Jacobs, C. S., Keihm, S., et al. 2007, IEEEP, 95, 2180
Barnard, E. E. 1891a, AJ, 11, 42
Barnard, E. E. 1891b, MNRAS, 52, 419
Barnard, E. E. 1908a, AN, 177, 145
Barnard, E. E. 1908b, MNRAS, 68, 360
Barnard, E. E. 1910, AJ, 26, 79
Barnard, E. E. 1912, AJ, 27, 116
Barnard, E. E. 1913a, AJ, 28, 1
Barnard, E. E. 1913b, AN, 194, 333
Barnard, E. E. 1914, AN, 198, 223
Barnard, E. E. 1915, AJ, 29, 33
Barnard, E. E. 1916, AJ, 30, 33
Barnard, E. E. 1918, AJ, 31, 49
Barnard, E. E. 1927, AJ, 37, 157
Bierman, G. J. 1977, Factorization Methods for Discrete Sequential Estimation (New York: Academic Press)
Bobone, J. 1953, AJ, 58, 172
Bosh, A. S., Rivkin, A. S., Percival, J. W., Taylor, M., & van Citters, G. W. 1997, Icar, 129, 555
Bowell, E. 1988, private communication
Campbell, J. K., & Anderson, J. D. 1989, AJ, 97, 1485
Carlsberg Meridian Cat 1999, Observations of Positions of Stars and Planets — May 1984 to May 1998, at La Palma No. 1–11 (Copehagen University Observatory, Royal Greenwich Observatory, and Real Instituto y Observatorio de la Armada en San Fernando)
Chernykh, L. I., & Chernykh, N. S. 1971, BITA, 12, 739
Christie, W. 1909, Greenwich Obs., 69, G197
Christie, W. 1910, Greenwich Obs., 70, G181
Christie, W. 1912, Greenwich Obs., 72, C119
Chugunov, I. G. 1981, IzEhn, 47, 111
Chugunov, I. G., & Nefedev, Y. A. 1980, ATsir, 1114, 7
Colwell, J. E., Cooney, J. H., Esposito, L. W., & Sremčević, M. 2009, Icar, 200, 574

Common, A. A. 1879, MNRAS, 40, 93
Corlies, P., Hayes, A. G., Birch, S. P. D., et al. 2017, GeoRL, 44, 11754
Debehogne, H. 1979, BuAst, 9, 68
Debehogne, H. 1981, IAUC, 3629, 3
Debehogne, H. 1982, IAUC, 3707, 3
Debehogne, H. 1984, BuAst, 9, 299
Dermott, S. F., & Murray, C. D. 1981, Icar, 48, 12
Dollfus, A. 1979, A&A, 75, 204
Dourneau, G., Bec-Borsenberger, A., & LeCampion, J.-F. 1991, Astrometric Observations of Phoebe, NSDB Data Set so0019, http://nsdb.imcce.fr/nsdb/home.html
Dourneau, G., Dulou, M. R., & Le Campion, J. F. 1985, A&A, 142, 91
Dourneau, G., Le Campion, J. F., & Dulou, M. R. 1989, AJ, 98, 716
Dourneau, G., Veillet, C., Dulou, M. R., & Le Campion, J. F. 1986, A&A, 160, 280
Durante, D., Hemingway, D. J., Racioppa, P., Iess, L., & Stevenson, D. J. 2019, Icar, 326, 123
Efroimsky, M., & Lainey, V. 2007, in AIP Conf. Ser. 886, New Trends in Astrodynamics and Applications III, ed. E. Belbruno (Melville, NY: AIP), 131
Elliot, J. L., Bosh, A. S., Cooke, M. L., et al. 1993, AJ, 106, 2544
Fienga, A., Arlot, J.-E., Baron, N., et al. 2002, A&A, 391, 767
Filippov, Y. K. 2001, Observations made at Golosseevo-Kiev (1963-1984), NSDB Data Set sm0031, http://nsdb.imcce.fr.nsdb/home.html
Fimmel, R. O., Van Allen, J., & Burgess, E. 1980, Pioneer First to Jupiter, Saturn, and Beyond, NASA SP 446 (Washington, DC: National Aeronautics and Space Administration)
Folkner, W. M. 1994, Effect of Uncalibrated Particles on Doppler Tracking, Interoffice Memo 335.1-94-005 (internal document) (Pasadena, CA: Jet Propulsion Laboratory)
Fortney, J. J., & Hubbard, W. B 2003, Icar, 164, 228
French, R. G., McGhee, C. A., Dones, L., & Lissauer, J. L. 2003, Icar, 162, 143
French, R. G., McGhee, C. A., Frey, M., et al. 2006, PASP, 118, 246
French, R. G., McGhee-French, C. A., Lonergan, K., et al. 2017, Icar, 290, 14
French, R. G., Nicholson, P. D., Cooke, M. L., et al. 1993, Icar, 103, 163
Giorgini, J. D., Yeomans, D. K., Chamberlin, A. B., et al. 1996, BAAS, 28, 1158
Gladman, B. J., Kavelaars, J. J., Holman, M., et al. 2000, Icar, 147, 320
Godard, M. H. 1919, JO, 3, 29
Gomes-Júnior, A. R., Assafin, M., Vieira-Martins, R., et al. 2015, A&A, 580, A76
Grosheva, E. A., Izmailov, I. S., & Kisseleva, T. P. 2011, SoSyR, 45, 523
Hall, A., Jr., Burton, H. E., Lyons, U. S., et al. 1954, Pub. U. S. Nav. Obs., 2nd. Ser., XVII, 93
Harper, D., Beurle, K., Williams, I. P., et al. 1999, A&AS, 136, 257
Harper, D., Murray, C. D., Beurle, K., et al. 1997, A&AS, 121, 65
Harper, D., & Taylor, D. B. 1994, A&A, 284, 619
Harris, H. 2007–2016, FASTT Astrometric Observations (2007-2016), http://www.nofs.navy.mil/data/plansat.html
Hatanaka, Y. 1995, PNAOJ, 4, 23
Hedman, M. M., & Nicholson, P. D. 2014, MNRAS, 444, 1369
Hedman, M. M., & Nicholson, P. D. 2016, Icar, 279, 109
Helled, R. 2011, ApJL, 735, L16
Herald, D., Gault, D., Anderson, R., et al. 2020, MNRAS, 499, 4570
Hubbard, W. B., Dougherty, M. K., Gautier, D., & Jacobson, R. 2009, in Saturn from Cassini-Huygens, ed. M. K. Dougherty et al. (Dordrecht: Springer), 75
Hubbard, W. B., Porco, C. C., Hunten, D. M., et al. 1993, Icar, 103, 215
Hussey, W. J. 1902, LicOB, 17, 139
Hussey, W. J. 1903, LicOB, 34, 34
Hussey, W. J. 1905, LicOB, 68, 71
Iess, L., Militzer, B., Kaspi, Y., et al. 2019, Sci, 364, 1052
Iess, L., Stevenson, D. J., Parisi, M., et al. 2014, Sci, 344, 78
Innes, R. T. A. 1908, MNRAS, 68, 32
Izhakevich, E. M. 1991, Position Photographic Observations of Satellites of Saturn in the Main Astronomical Observatory of Ukrainian Academie of Science in 980, Scientific Paper Deposited in all-Russian Institute of Scientific and Technical Information. No. 4553-B911
Izhakevich, E. M. 2001, Observations made at Golosseevo-Kiev (1976-1984), NSDB Data Set sm0032, http://nsdb.imcce.fr/nsdb/home.html
Jacobson, R. A. 1998, A&AS, 128, 7
Jacobson, R. A. 2004, AJ, 128, 492
Jacobson, R. A. 2010, AJ, 139, 668
Jacobson, R. A., Antreasian, P. G., Bordi, J. J., et al. 2006a, AJ, 132, 2520
Jacobson, R. A., Spitale, J., Porco, C. C., & Owen, W. M., Jr. 2006b, AJ, 132, 711
Jones, D. 1999, Phoebe observations at La Palma, NSDB Data Set so0005, http:/nsdb.imcce.fr/nsdb/home.html
Khrutskaya, E. V., Kisseleva, T. P., Izmailov, I. S., Khovrichev, M. Y., & Berezhnoy, A. A. 2009, SoSyR, 43, 285
Kiladze, R. I. 1969, Bull. Abast. Astrophys. Obs., 37, 151
Kisseleva, T. P. 2009, Observations Made at Pulkovo (2002-2008), NSDB Data Set sm0058, http://nsdb.imcce.fr/nsdb/home.html
Kisseleva, T. P., Chanturia, S. M., Lepeshenkova, A., et al. 1987, AbaOB, 62, 117
Kisseleva, T. P., & Izmailov, I. S. 2000, IzGla, 214, 333
Kisseleva, T. P., & Kalinitchenko, O. A. 1998, IzGla, 213, 122
Kisseleva, T. P., & Kalinitchenko, O. A. 2000, IzGla, 214, 344
Kisseleva, T. P., & Kalinitchenko, O. A. 2002, IzGla, 216, 185
Kisseleva, T. P., Kisselev, A. A., Khrutskaya, E. V., & Kalinitchenko, O. A. 1996, IzGla, 210, 76
Kisseleva, T. P., Koroleva, L. S., & Panova, G. V. 1975, BITA, 14, 60
Kisseleva, T. P., Panova, G. V., & Kalinichenko, O. A. 1977, IzPul, 195, 49
Kitkin, V. N. 1985, Observations of Saturn's satellites made at the Engelhardt Astronomical Observatory and the Zelenchuksyaya Astronomical Station in 1982-1984, Tech. rep. (Kazan: Kazan Univ.)
Kitkin, V. N., & Chugunov, I. G. 1980, Photographic observations of Saturn's satellites at the Engelhardt Astronomical Observatory in January–May 1980, Tech. Rep. (Saransk: Mordovsk Univ.)
Kitkin, V. N., & Chugunov, I. G. 1982, Photographic observations of Saturn's satellites at the Engelhardt Astronomical Observatory in 1981, Tech. Rep. (Saransk: Mordovsk Univ.)
Kowalski, R. A. 2001, Minor Planet Circ. No. 44181 (Cambridge, MA: Smithsonian Astrophysical Observatory)
Krasinsky, G. 2000, private communication
Krogh, F. T., Ng, E. W., & Snyder, W. V. 1982, CeMec, 26, 395
Lainey, V., Gomez Casajus, L., Fuller, J., et al. 2020, NatAs, 4, 1053
Lainey, V., Jacobson, R. A., Tajeddine, R., et al. 2017, Icar, 281, 286
Lamy, P., & Mauron, N. 1980, IAUC, 3491, 3
Laques, P., Wierick, G., Lelievre, G., & Lecacheux, J. 1980, IAUC, 3483, 1
Larson, S. M., & Fountain, J. W. 1981, IAUC, 3602
Lawson, C. L., & Hanson, R. J. 1974, Solving Least Squares Problems (Englewood Cliffs, NJ: Prentice-Hall, Inc.)
Ledovskaya, I. V., Jockers, K., Karpov, N. V., & Sergeev, A. 1999, Kinematika Iphisika Nebesnykh Tel, 15, 483
Leliévre, G. 1980, IAUC, 3545, 1
Levitskaya, T. I. 1979, ATsir, 1084, 6
Lindegren, L. 1977, A&A, 57, 55
Lorenz, R. D., Turtle, E. P., Barnes, J. W., et al. 2018, JHATD, 34, 1
Mackenzie, R. 2006, Numerical Limitations to Computed Doppler Precision, Interoffice Memo 343J-06-017 (internal document) (Pasadena, CA: Jet Propulsion Laboratory)
Mackenzie, R. A., & Folkner, W. M. 2006, Applying Appropriate Weights to Doppler Data, Interoffice Memo 343J-06-034 (internal document) (Pasadena, CA: Jet Propulsion Laboratory)
Mankovich, C., Marley, M. S., Fortney, J. J., & Movshovitz, N. 2019, ApJ, 871, 1
Martinka, S., & Pascu, D. 1998, private communication
McGhee, C. A., Nicholson, P. D., French, R. G., & Hall, K. J. 2001, Icar, 152, 282
Mignard, F. 1979, M&P, 20, 301
Monet, A. 2005–2007, FASTT Sstrometric Observations (2005-2007), http://www.nofs.navy.mil/data/plansat.html
Morrison, D. 1982, Voyages to Saturn, NASA SP 451 (Washington, DC: National Aeronautics and Space Administration)
Movshovitz, N., Fortney, J. J., Mankovich, C., Thorngren, D., & Helled, R. 2020, AJ, 891, 109
Moyer, T. D. 1968, Supporting Research and Advanced Development, Space Programs Summary 37-49 (Pasadena, CA: Jet Propulsion Laboratory), 40
Moyer, T. D. 2000, Formulation for Observed and Computed Values of Deep Space Network Data Types for Navigation, Deep Space Communications and Navigation Series: Monograph 2 (Pasadena, CA: Jet Propulsion Laboratory)
MPC 2000–2019, Circular No. 38967, 40910, 40911, 41261, 41449, 41635, 41637, 41830, 42025, 43757, 43830, 44181, 44182, 47291, 47504, 50459, 50594, 53171, 53464, 53629, 53948, 54163, 55508, 55975, 55976, 56148, 56608, 56609, 56794, 56953, 57946, 57947, 58097, 58523, 58764, 59029, 59305, 59581, 59860, 60086, 61685, 61686, 61978, 62254, 62566, 62864, 62865, 63123, 63363, 63584, 64482, 64749, 65036, 65325, 65628, 65920, 66188, 66450, 66686, 68212, 68669, 69202, 69724, 70193, 70653, 73667, 74025, 74380, 74811, 75145, 75400, 75593, 75849, 78327, 78784, 79140, 79473, 79746, 79971, 82023, 82866, 83713, 83714, 87200, 88086, 88462,

90446, 93768, 94438, 97001, 99950, 100689, 101342, 104989, 105715, 115066 (Cambridge, MA: Minor Planet Center, Smithsonian Astrophysical Observatory)
Mulholland, J. D., & Shelus, P. J. 1980, AJ, 85, 1112
Mulholland, J. D., Shelus, P. J., & Abbot, R. I. 1976, AJ, 81, 1007
Murray, C. D., & Dermott, S. F. 1999, Solar System Dynamics (Cambridge: Cambridge Univ. Press)
Nicholson, P. D. 1994, private communication
Nicholson, P. D. 2000, private communication
Nicholson, P. D., Cooke, M. L., & Pelton, E. 1990, AJ, 100, 1339
Nicholson, P. D., Showalter, M. R., Dones, L., et al. 1996, Sci, 272, 509
Nimmo, F., Barr, A. C., Běhounková, M., & McKinnon, W. B. 2018, in Enceladus and the Icy Moons of Saturn, ed. P. M Schenk et al. (Tucson, AZ: The Univ. of Arizona Press), 387
Nimmo, F., Bills, B. G, & Thomas, P. C 2011, JGR, 116, E11001
Noyelles, B., Vienne, A., & Descamps, P. 2003, A&A, 401, 1159
Null, G. W., Lau, E. L., Biller, E. D., & Anderson, J. D. 1981, AJ, 86, 456
Oberti, P., Veillet, C., & Catullo, V. 1989, A&AS, 80, 289
Owen, W. M. 2018, private communication
Park, R. S., Folkner, W. M., Williams, J. G., & Boggs, D. H. 2021, AJ, 161, 105
Pascu, D. 1982, private communication
Pascu, D., & Seidelmann, P. K. 1981, IAU Circ. No. 3619
Peng, Q. Y., Vienne, A., & Shen, K. X. 2002, A&A, 383, 296
Peng, Q. Y., Vienne, A., Wu, X. P., Gan, L. L., & Desmars, J. 2008, AJ, 136, 2214
Peng, Q. Y., Wang, N., Vienne, A., et al. 2015, MNRAS, 449, 2638
Peng, Q. Y., & Zhang, Q. F. 2006, MNRAS, 366, 208
Perrine, C. 1904, LicOB, 3, 52
Perrine, C., Albrecht, S., & Smith, E. 1909, LicOB, 5, 106
Peters, C. F. 1973, AJ, 78, 957
Peters, C. F. 1981, A&A, 104, 37
Pickering, E. 1906a, Observations of Phoebe during 1905, Harv. Coll. Obs. Circ. No. 109
Pickering, E. 1906b, Observations of Phoebe in May and June, 1906, Harv. Coll. Obs. Circ. No. 118
Pickering, E. 1906c, Observations of Phoebe in August and September, 1906, Harv. Coll. Obs. Circ. No. 119
Pickering, W. 1905a, Annals Harvard Col. Obs., LIII, 45
Pickering, W. 1905b, Annals Harvard Col. Obs., LIII, 85
Pickering, W. 1908, Annals Harvard Col. Obs., LX, 45
Porco, C. C., Baker, E., Barbara, J., et al. 2005, Sci, 307, 1226
Porco, C. C. & the Cassini Imaging Team 2004, IAUC, 8432, 1
Qiao, R. C., Shen, K. X., Harper, D., & Liu, J. R. 2004, A&A, 422, 377
Qiao, R. C., Shen, K. X., Liu, J. R., & Harper, D. 1999, A&AS, 137, 1
Qiao, R. C., Tang, Z. H., Shen, K. X., et al. 2006, A&A, 454, 379
Qiao, R. C., Xi, X. J., Dourneau, G., et al. 2011, MNRAS, 413, 1079
Rapaport, M. 1989, private communication
Rapaport, M. 1992, private communication
Rapaport, M., Teixeira, R., Le Campion, J. F., et al. 2002, A&A, 383, 1054
Reitsema, H. J. 1981, Icar, 48, 23
Retisema, H. J., Smith, B. A., & Larson, S. M. 1980, IAUC, 3466, 2
Richmond, M., & Nicholson, S. 1943, AJ, 50, 163
Roemer, E., & Lloyd, R. 1966, AJ, 71, 443
Rohde, J. 1994, private communication
Rohde, J. R., Ianna, P. A., Stayton, L. C., & Levinson, F. H. 1982, AJ, 87, 698
Rohde, J. R., & Pascu, D. 1993, BAAS, 25, 1235
Rohde, J. R., & Pascu, D. 1994, BAAS, 26, 1024
Seidelmann, P. K., Harrington, R. S., Pascu, D., et al. 1981, Icar, 47, 282
Seitzer, P., & Ianna, P. A. 1980, AJ, 85, 1117
Seitzer, P., Ianna, P. A., & Levinson, F. 1979, AJ, 84, 877
Shelus, P. 1998, private communication
Shen, K. X. 1988, private communication
Simpson, R. A., Tyler, G. L., & Holberg, J. B. 1983, AJ, 88, 1531
Sinclair, A. T. 1974, MNRAS, 169, 591
Sinclair, A. T. 1977, MNRAS, 180, 447
Soulie, G. 1968, JO, 51, 315
Soulie, G. 1972, A&AS, 6, 311
Soulie, G. 1975, A&AS, 22, 49
Soulie, G. 1978, A&AS, 33, 257
Soulie, G., Dupouy, T., & Broqua, D. 1981, A&AS, 43, 147
Spilker, L. 2019, Sci, 364, 1046
Standish, E. M. 1996, Astrographic Positions of the Satellites of Jupiter, Saturn, and Uranus, IOM 312.1-96-020 (Pasadena, CA: Jet Propulsion Laboratory)
Stone, R. C. 2000, AJ, 120, 2124
Stone, R. C. 2001, AJ, 122, 2723
Stone, R. C. 2001–2005, FASTT Astrometric Observations (2001-2005), http://www.nofs.navy.mil/data/plansat.html
Stone, R. C., & Harris, F. H. 2000, AJ, 119, 1985
Strugnell, P. R., & Taylor, D. B. 1990, A&AS, 83, 289
Struve, G. 1933, Veroff. Berlin Babelsberg, 6, Ei–E44
Struve, H. 1898, Publ. l'Obs. Cent. Nicolas., ser. 2, Vol. 11 (St. Petersburg: Imprimerie de L'Académie Impériale des Sciences)
Taylor, D. B., & Sinclair, A. T. 1985, A&AS, 61, 221
Thomas, P. C. 2010, Icar, 208, 395
Thomas, P. C., Burns, J. A., Hedman, M., et al. 2013, Icar, 226, 999
Thomas, P. C., Tajeddine, R., Tiscareno, M. S., et al. 2016, Icar, 264, 37
Thomas, P. C., Tiscareno, M. S., & Helfenstein, P. 2018, in Enceladus and the Icy Moons of Saturn, ed. P. M Schenk et al. (Tucson, AZ: The University of Arizona Press), 387
Tiscareno, M. S., Burns, J. A., Nicholson, P. D., Hedman, M. M., & Porco, C. C. 2007, Icar, 189, 14
Tolbin, S. V. 1991a, All-Russian Institude of Scientific and Technical Information, 3078-B91, 1
Tolbin, S. V. 1991b, All-Russian Institute of Scientific and Technical Information, 3077-B91, 1
Tortora, P., Zannoni, M., Hemingway, D., et al. 2016, Icar, 264, 264
USNO 1877-87, Astronomical and Meteorological Observations Made During the Years 1874–1883 (Washington, DC: U.S. Naval Observatory)
USNO 1887,1889-93, Astronomical and Meteorological Observations Made During the Years 1883-1889 (Washington, DC: U.S. Naval Observatory)
USNO 1911, Pub. U. S. Naval Observatory, VI., Ser. 2 (Washington, DC: U.S. Naval Observatory)
USNO 1929, Pub. U. S. Naval Observatory, XII., Ser. 2 (Washington, DC: U.S. Naval Observatory)
van Biesbroeck, G. 1922, AJ, 34, 167
van Biesbroeck, G. 1944, AJ, 50, 184
van Biesbroeck, G. 1956, AJ, 62, 136
van Biesbroeck, G. 1958, AJ, 63, 147
van Biesbroeck, G., Vesely, C., Aksnes, K., & Marsden, B. 1976, AJ, 81, 122
Vass, G. 1997, RoAJ, 7, 45
Veiga, C. H., & Vieira Martins, R. 1999, A&AS, 139, 305
Veiga, C. H., & Vieira Martins, R. 2000, A&AS, 143, 405
Veiga, C. H., Vieira Martins, R., & Andrei, A. H. 2000, A&AS, 142, 81
Veiga, C. H., Vieira Martins, R., Vienne, A., Thuillot, W., & Arlot, J. 2003, A&AS, 400, 1095
Veillet, C. 1980, IAUC, 3470, 2
Veillet, C., & Dourneau, G. 1992, A&AS, 94, 291
Vienne, A., Thuillot, W., Veiga, C. H., Arlot, J., & Vieira Martins, R. 2001, A&A, 380, 727
von Engelhardt, B. 1887, AN, 117, 9
von Engelhardt, B. 1888, AN, 119, 315
von Engelhardt, B. 1890, AN, 126, 227
Wahl, S. M., Hubbard, W. B., & Militzer, B. 2017, Icar, 282, 183
Walker, R. L., Christy, J. W., & Harrington, R. S. 1978, AJ, 83, 838
Whipple, A. 1996, private communication
Whipple, A. L. 1993, private communication
Whipple, A. L. 1995, private communication
Yoder, C. F. 1995, in Global Earth Physics: A Handbook of Physical Constants, ed. T. J Ahrens (Washington, DC: American Geophysical Union), 1
Zannoni, M., Hemingway, D., Gomez Casajus, L., & Tortora, P. 2020, Icar, 345, 113713